

# Relativistic Mean-Field Treatment of Pulsar Kick from Neutrino Propagation in Magnetized Proto-Neutron

Tomoyuki Maruyama,<sup>1,2,3</sup> Nobutoshi Yasutake,<sup>4</sup> Myung-Ki Cheoun,<sup>5,3</sup>

Jun Hidaka,<sup>3</sup> Toshitaka Kajino,<sup>3,6</sup> Grant J. Mathews,<sup>7</sup> and Chung-Yeol Ryu<sup>5</sup>

<sup>1</sup>*College of Bioresource Sciences, Nihon University, Fujisawa 252-8510, Japan*

<sup>2</sup>*Advanced Science Research Center,*

*Japan Atomic Energy Research Institute, Tokai 319-1195, Japan*

<sup>3</sup>*National Astronomical Observatory of Japan,*

*2-21-1 Osawa, Mitaka, Tokyo 181-8588, Japan*

<sup>4</sup>*Research Institute for the Early Universe, University of Tokyo,*

*Hongo 7-3-1, Bunkyo-ku, Tokyo 113-0033, Japan*

<sup>5</sup>*Department of Physics, Soongsil University, Seoul, 156-743, Korea*

<sup>6</sup>*Department of Astronomy, Graduate School of Science,*

*University of Tokyo, Hongo 7-3-1, Bunkyo-ku, Tokyo 113-0033, Japan*

<sup>7</sup>*Center of Astrophysics, Department of Physics,*

*University of Notre Dame, Notre Dame, IN 46556, USA*

(Dated: July 27, 2021)

## Abstract

We make a perturbative calculation of neutrino scattering and absorption in hot and dense hyperonic neutron-star matter in the presence of a strong magnetic field. We calculate that the absorption cross-sections in a fully relativistic mean-field theory. We find that there is a remarkable angular dependence, *i.e.* the neutrino absorption strength is reduced in a direction parallel to the magnetic field and enhanced in the opposite direction. This asymmetry in the neutrino absorption is estimated to be as much as 2.2 % of the entire neutrino momentum for an interior magnetic field of  $\sim 2 \times 10^{17}$  G. The pulsar kick velocities associated with this asymmetry are shown to be comparable to observed velocities.

PACS numbers: 25.30.Pt, 21.65.Cd, 24.10.Jv, 95.85.Sz, 97.60.Jd,

## I. INTRODUCTION

Hot and dense hadronic matter is a topic of considerable current interest in nuclear and particle physics as well as astrophysics because of its associated exotic phenomena. In particular, many studies have addressed the possible exotic phases of high density matter. Neutron stars are thought to be the most realistic possible sites to study the physics of high density matter. For example, the possible existence of an anti-kaon condensation in neutron stars has been suggested [1], and the possible implications for its astrophysical phenomena have been widely discussed [2–5].

These discussions, however, heavily depend upon the nuclear-matter equation of state (EOS), which governs both the static and dynamic properties of neutron stars. Hence, many papers [6–13] have been devoted to the study of the neutron-star EOS. In particular, the thermal evolution of neutron stars by neutrino emission is a topic of considerable interest [14–20] regarding the dynamical evolution of neutron stars. For example, Reddy *et al.* [21] studied neutrino propagation in proto-neutron stars (PNSs) as a means to examine the hyperon phase in the high density region.

On the other hand, since the discovery of magnetars [22, 23], magnetic fields are thought to play an important role in many astrophysical phenomena such as the development of asymmetry in supernova (SN) remnants. Indeed, strong magnetic fields turn out to be a crucial ingredient for the still poorly understood mechanism to produce non-spherical SN explosions, pulsar kicks [24], i.e. the high velocity [25] that some PNSs receive at birth.

Although several post-collapse instabilities have been studied as a possible source of non-spherical explosions and pulsar kicks, the unknown origin of the initial asymmetric perturbations and the uncertainties in the numerical simulations make this possibility difficult to unambiguously verify [26, 27]. Another viable candidate is the possibility of asymmetric neutrino emission either as a result of parity violation in the weak interaction [28, 29] or as a result of an asymmetric magnetic field [30] in strongly magnetized PNSs.

In this work, we take the asymmetric neutrino emission as one of the main reasons for the asymmetric phenomena observed in the PNS. This asymmetric neutrino emission is assumed be caused by the two processes; one is the asymmetric production inside PNSs; and the other is the damping of the neutrino luminosity through neutrino absorption in the nuclear medium.

The direct and modified URCA processes may play a role in neutrino emission, but the main effect of these processes is in the neutron-star cooling [14, 31], where in-medium effects play an important role [32, 33]. Of course, a strong magnetic field leads to an angular-dependence of the neutrino production in the URCA process because of the spin polarization of electrons and positrons in matter [34, 35]. Nevertheless, we assume here that the URCA process is not important in the PNS stage.

Other effects, such as the Landau levels due to the magnetic field [36, 37], the angular dependence of the neutrino production caused by a possible pion condensation phase [38, 39], and a possible quark-matter color-super conducting phase [40] *etc* are also assumed to be small in this work.

Over a decade ago, Lai *et al.* [41, 42] calculated the neutrino-nucleon scattering during neutrino propagation inside a neutron star in the context of a non-relativistic framework [41]. Within that approximation they showed that even a  $\sim 1\%$  asymmetry in the total neutrino luminosity of  $\sim 10^{53}$  ergs could be enough to explain the observed pulsar kick velocities.

Kusenko, Segre and Vilenkin [43] criticized this conclusion and theoretically showed that the asymmetry in the neutrino scattering cross-section does not lead to an asymmetry in the neutrino emission if the system is in complete thermodynamic equilibrium. However, they only considered only neutrino-neutron collisions and neglected the Fermi-Dirac statistics. Hence, their proof is only applicable in the very low-density region. Furthermore, neutrino scattering inside dense nuclear matter does not play a role in either the thermal evolution or the propagation of the non-equilibrium part of the neutrinos. On the other hand, the absorption part of the collisions may make a large contribution to the asymmetry [44]. That is what we demonstrate here.

On the other hand, the past decades have seen many successes in the relativistic treatment of the nuclear many-body problem. The relativistic framework has several advantages [45, 46]. Among them this formalism provides a useful Dirac phenomenology for the description of nucleon-nucleus scattering [47, 48], a natural means to incorporate the spin-orbit force [46], and a reliable means to compute the structure of extreme nuclei [49]. These results have shown that there are large attractive scalar and repulsive vector fields, and that the nucleon effective mass becomes small in the nuclear medium. This mechanism may drive the self-suppression mechanism of kaon-condensation in nuclear matter, and may lead to a stable kaon condensation phase in neutron stars (NSs) [7].

In Ref. [44] we reported results for the first time on the neutrino absorption cross-sections in hot dense magnetized NS matter calculated in a fully relativistic mean field (RMF) theory [45, 46] including hyperons. In that work we took into account the Fermi motion of baryons and electrons, their recoil effects, distortion effects of the Fermi spheres by the magnetic field, and effects from the energy difference of the mean field between initial and final baryons in a fully relativistic framework. We found that even a few percent breaking of isotropic symmetry in the neutrino absorption cross-section may cause an asymmetric emissions of neutrinos from PNSs.

In this paper, we provide more detailed explanations of the neutrino scattering and absorption cross-sections in magnetized NS matter in the context of RMF theory. We then solve the Boltzmann equation for neutrino transport in a 1D model and discuss implications of our numerical results for pulsar kicks. In particular, we focus on the collision between a neutrino and a particle in nuclear matter in the presence of a strong magnetic field and a core temperature of 20 – 40MeV. Two-baryon process are not taken into account in the present PNS calculation since they only play an important role at low temperature ( $\sim$  a few MeV) [31].

In Sec. II we introduce our EOS for nuclear matter based upon the RMF theory. In Sec. III we explain the neutrino scattering and absorption cross-sections in baryonic matter in the presence of strong magnetic fields. Numerical results and detailed discussions of neutrino reactions and propagation in baryonic matter at finite temperature are presented in Sec. IV. Summaries are given in Sec. V with further arguments on the associated pulsar kicks of magnetized PNSs. Finally, in Sec. VI, as topics for future work, we discuss other plausible characteristics of PNS interiors that may affect the pulsar kicks.

## II. NEUTRON-STAR MATTER IN THE RELATIVISTIC MEAN-FIELD APPROACH

In this work we calculate neutrino cross-sections in neutron-star matter in the RMF approach. For this purpose we define the Lagrangian density as

$$\mathcal{L} = \mathcal{L}_{Lep} + \mathcal{L}_{RMF} + \mathcal{L}_{Mag} + \mathcal{L}_W, \quad (1)$$

where the first, second, third and fourth terms are the lepton, RMF, magnetic, and weak interaction parts, respectively. We consider NS matter including nucleons, Lambdas, electrons and electro-neutrinos ( $\nu_e$ ). Detailed expressions for the magnetic and weak parts are explained in the next section.

The lepton and RMF parts of the Lagrangian density utilized in this work are given as

$$\begin{aligned} \mathcal{L}_{Lep} &= \bar{\psi}_\nu i\gamma_\mu \partial^\mu \psi_\nu + \bar{\psi}_e (i\gamma_\mu \partial^\mu - m_e) \psi_e, \\ \mathcal{L}_{RMF} &= \bar{\psi}_N (i\gamma_\mu \partial^\mu - M_N) \psi_N + g_\sigma \bar{\psi}_N \psi_N \sigma + g_\omega \bar{\psi}_N \gamma_\mu \psi_N \omega^\mu \\ &\quad + \bar{\psi}_\Lambda (i\gamma_\mu \partial^\mu - M_\Lambda) \psi_\Lambda + g_\sigma^\Lambda \bar{\psi}_\Lambda \psi_\Lambda \sigma + g_\omega^\Lambda \bar{\psi}_\Lambda \gamma_\mu \psi_\Lambda \omega^\mu \\ &\quad - \tilde{U}[\sigma] + \frac{1}{2} m_\omega^2 \omega_\mu \omega^\mu - \frac{C_{IV}}{2M_N^2} \bar{\psi}_N \gamma_\mu \tau_a \psi_N \bar{\psi}_N \gamma^\mu \tau_a \psi_N, \end{aligned} \quad (2)$$

$$(3)$$

where  $\psi_\nu$ ,  $\psi_e$ ,  $\psi_N$ ,  $\psi_\Lambda$ ,  $\sigma$ , and  $\omega$  are the electron neutrino, and electron, nucleon, Lambda, sigma-meson and omega-meson fields, respectively, with corresponding masses  $m_e$ ,  $M_N$ ,  $M_\Lambda$ , and  $m_\omega$ .  $\tilde{U}[\sigma]$  is the self-energy potential of the scalar mean-field given in Refs. [7, 50]. The last term describes the vector isovector interaction between two nucleons, which is equivalent to  $\rho$ -meson exchange [45]. We adopt natural units, *i.e.*  $\hbar = c = 1$ .

From the Euler-Lagrange equation of the above Lagrangian, the Dirac spinor of the baryon  $u_b(\mathbf{p}, s)$  is obtained as a solution to the following equation

$$[\not{p} - M_b^* - U_0(b)\gamma_0] u_b(\mathbf{p}, s) = 0, \quad (4)$$

where  $U_0(b)$  is the time component of the mean-field vector potential. We hereafter introduce the Feynman dagger  $\not{p} \equiv \gamma_\mu p^\mu$  for convenience. The baryon effective masses  $M_b^*$  are given by

$$\begin{aligned} M_N^* &= M_N - U_s(N), \\ M_\Lambda^* &= M_\Lambda - U_s(\Lambda), \end{aligned} \quad (5)$$

with the scalar mean-field potentials

$$U_s(N) = g_\sigma \langle \sigma \rangle, \quad U_s(\Lambda) = g_\sigma^\Lambda \langle \sigma \rangle. \quad (6)$$

The scalar mean-field  $\langle \sigma \rangle$  is given by

$$\frac{\partial}{\partial \langle \sigma \rangle} \tilde{U}[\langle \sigma \rangle] = g_\sigma [\rho_s(p) + \rho_s(n)] + g_\sigma^\Lambda \rho_s(\Lambda), \quad (7)$$

with the scalar densities

$$\rho_s(b) \equiv \frac{2}{(2\pi)^3} \int d^3\mathbf{p} \left[ n_b^{(+)}[e_b^{(+)}(\mathbf{p})] + n_b^{(-)}[e_b^{(-)}(\mathbf{p})] \right] \frac{M_b^*}{E_b^*(\mathbf{p})}. \quad (8)$$

Here,  $e_b^{(\pm)}$  are the single particle (+) and antiparticle (-) energies,  $E_b^*(\mathbf{p}) = \sqrt{\mathbf{p}^2 + M_b^{*2}}$ , and the Fermi distributions,  $n_b^{(\pm)}(e_b^{(\pm)})$ , are defined as usual,

$$n_b^{(\pm)}(e_b^{(\pm)}) = \frac{1}{1 + \exp[(e_b^{(\pm)} \pm \varepsilon_b)/T]}, \quad (9)$$

in terms of the temperature  $T$  and the chemical potential  $\varepsilon_b$ .

In addition, the baryon single-particle energies are written as  $e_b^{(\pm)}(\mathbf{p}) = E_b^*(\mathbf{p}) \pm U_0(b)$ , with the  $U_0(b)$  calculated as

$$U_0(p) = \frac{g_\omega}{m_\omega^2} \{g_\omega(\rho_p + \rho_n) + g_\omega^\Lambda \rho_\Lambda\} + \frac{C_{IV}}{M_N^2}(\rho_p - \rho_n), \quad (10)$$

$$U_0(n) = \frac{g_\omega}{m_\omega^2} \{g_\omega(\rho_p + \rho_n) + g_\omega^\Lambda \rho_\Lambda\} - \frac{C_{IV}}{M_N^2}(\rho_p - \rho_n), \quad (11)$$

$$U_0(\Lambda) = \frac{g_\omega^\Lambda}{m_\omega^2} \{g_\omega(\rho_p + \rho_n) + g_\omega^\Lambda \rho_\Lambda\} \quad (12)$$

in terms of the proton, neutron and Lambda number densities,  $\rho_p$ ,  $\rho_n$  and  $\rho_\Lambda$ .

In this work, neutron-star matter at finite temperature includes protons, neutrons, Lambdas( $\Lambda$ s), electrons and neutrinos. These are constrained by the conditions of charge neutrality and beta equilibrium. Therefore, the proton number density is equal to the electron number density,  $\rho_p = \rho_e$ , and the chemical potentials obey the following condition

$$\varepsilon_n = \varepsilon_\Lambda = \varepsilon_p + \varepsilon_e. \quad (13)$$

The lepton fraction is also fixed as  $Y_L = (\rho_e + \rho_\nu)/\rho_B$  with  $\rho_B = \rho_p + \rho_n + \rho_\Lambda$ .

Since we focus only on the asymmetry of neutrino emission caused by the presence of a magnetic field and the existence of strange matter, we choose one parameter-set, PM1-L1

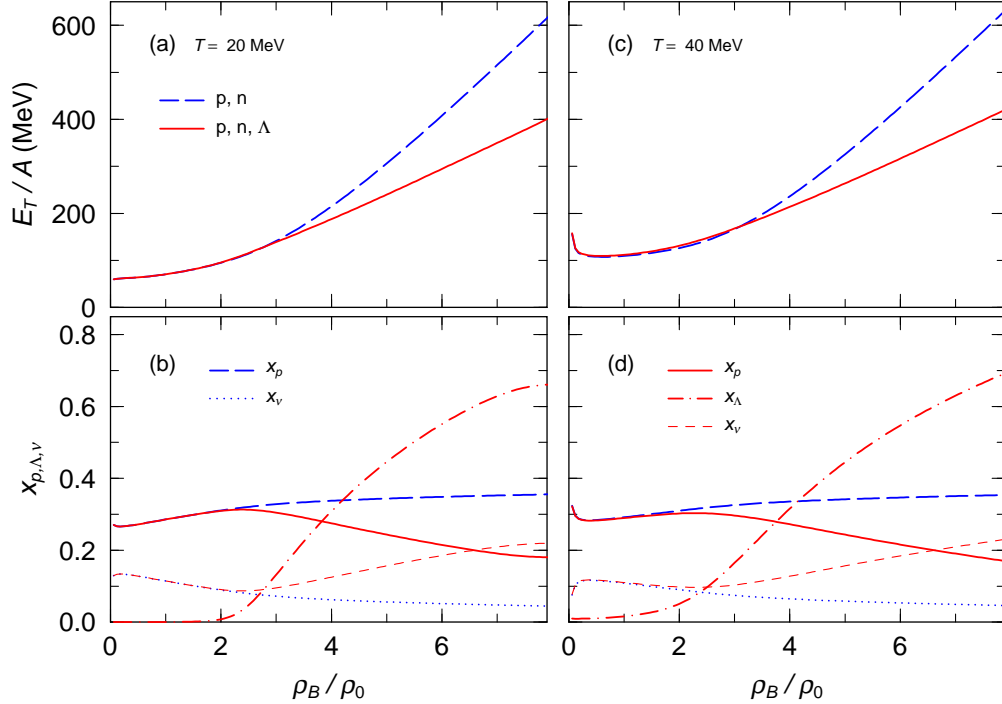


FIG. 1: (Color online) Upper panels (a) and (c) show the density dependence of the total energy per baryon  $E_T/A$  in neutron-star matter for  $T = 20$  MeV (a) and  $40$  MeV (c). Solid and long-dashed lines represent results with and without  $\Lambda$  particles. Lower panels (b) and (d) show number fractions of protons  $x_p$ ,  $\Lambda$  particles  $x_\Lambda$ , and neutrinos  $x_\nu$  for  $T = 20$  MeV (b) and  $40$  MeV (d). Solid, dot-long-dashed, and short-dashed lines represent proton, Lambda, and neutrino number fractions, respectively. Long-dashed and dotted lines represent the calculated proton and neutrino number fractions in a system without  $\Lambda$ s. In the present calculations we use the parameter-set PM1-L1 [51] for the RMF and the lepton fraction is set to  $Y_L = 0.4$ .

[51], in order not to distract the discussion. This parameter set gives the binding energy per baryon  $BE = 16$  MeV, a nucleon effective mass of  $M_N^*/M_N = 0.7$  and an incompressibility parameter of  $K = 200$  MeV at  $\rho_0 = 0.17 \text{ fm}^{-3}$  in nuclear matter. The sigma- and omega-Lambda couplings are  $2/3$  of those for the nucleon,  $g_{\sigma,\omega}^\Lambda = \frac{2}{3}g_{\sigma,\omega}$ . Similar relations are used in the quark meson coupling (QMC) model [52].

In Fig. 1 we show the energy per nucleon, which is a kind of the equation of state (EOS), in the upper panels (a and c) and the proton and Lambda fractions in the lower panels (b and d) at  $T = 20$  MeV (a and b) and  $T = 40$  MeV (c and d). In these calculations the lepton fraction is taken to be  $Y_L = 0.4$ . Solid and dashed lines represent the results for matter with

and without  $\Lambda$ s, respectively. Dot-dashed lines in the lower panels indicate the Lambda fraction, which appears when  $\rho_B \gtrsim 2\rho_0$  and significantly affects the EOS for  $\rho_B \gtrsim 3\rho_0$ .

Here we should comment about the anti-particle contribution. The density of anti-neutrinos is less than 0.5 % of the neutrino density when  $\rho_B = \rho_0$  and  $T = 40\text{MeV}$ . This ratio is much lower than other particles. With larger density and lower temperature, this ratio becomes smaller. Thus, anti-particles does not significantly contribute to the EOS or other observables as discussed below.

When Lambda particles are not included, the PM1-L1 EOS is sufficiently stiff [7] to allow a neutron star with mass larger than the value observed for PSR J1614-2230 of  $M = 1.97 \pm 0.04M_\odot$  [53]. When the Lambda particles are included, however, the EOS becomes softer and does not allow such a large maximum neutron-star mass. This could be resolved if we introduce additional repulsive force between  $\Lambda$ s [54] consistent with hypernuclear data. Another possibility would be introducing a repulsive three-body force.

In this paper, however, our goal is to explore the effects of magnetic fields in generating pulsar kicks and not to discuss the ambiguity of the mean-field EOS in regards to the maximum neutron-star mass. In this work, therefore, only the  $\Lambda$  particle is introduced as a hyperon. One could also introduce a Sigma ( $\Sigma$ ) mean-field in matter, which is repulsive [55] and appears at rather high density. However, its abundance fraction is small [56, 57]. Though the Xi ( $\Xi$ ) particle may be attractive [58], we do not have sufficient information about the Xi ( $\Xi$ ) particle and ignore its contribution.



### III. CROSS-SECTIONS FOR NEUTRINO REACTIONS IN MAGNETIZED PROTO-NEUTRON STAR MATTER

#### A. Dirac Wave Function in a Magnetic Field

We assume a uniform magnetic field along the  $z$ -direction  $\mathbf{B} = B\hat{z}$  with  $B \lesssim 10^{18}$  G. For this field strength the effect of the magnetic field on baryons is small enough to be treated perturbatively. The magnetic part of the Lagrangian density is written as

$$\mathcal{L}_{Mag} = \mathcal{L}_{BM} + \mathcal{L}_{eM}, \quad (14)$$

where the first and second terms describe the magnetic interactions of baryons and electrons, respectively.

Considering only the spin-interaction term, the baryon magnetic-interaction Lagrangian density can be written as

$$\mathcal{L}_{BM} = \sum_b \mu_b \bar{\psi}_b \sigma_{\mu\nu} \psi_b F^{\mu\nu} = \sum_b \mu_b \bar{\psi}_b \sigma_z \psi_b B \quad (15)$$

with the electromagnetic tensor given by  $F^{\mu\nu} = \partial^\mu A^\nu - \partial^\nu A^\mu$ , where  $A^\mu$  is the electromagnetic vector potential,  $\sigma_{\mu\nu} = [\gamma_\mu, \gamma_\nu]/2i$ ,  $\sigma_z = \text{diag}(1, -1, 1, -1)$  and  $\mu_b$  is the baryon magnetic moment. The baryon wave functions can be obtained by solving the following Dirac equation

$$[\not{p} - M_b^* - U_0(b)\gamma_0 - \mu_b B \gamma_0 \sigma_z] u_b(p, s) = 0. \quad (16)$$

The single particle energies  $e_b(\mathbf{p}, s)$  and the Dirac spinors in the limit of a weak magnetic field are given as

$$\begin{aligned} e_b(\mathbf{p}, s) &= \sqrt{p_z^2 + \left( \sqrt{\mathbf{p}_T^2 + M_b^{*2}} + \mu_b B s \right)^2} + U_0(b) \\ &\approx E_b^*(\mathbf{p}) + U_0(b) + \Delta E_b^*(\mathbf{p}) s \end{aligned} \quad (17)$$

with

$$\Delta E_b^*(\mathbf{p}) = \frac{\sqrt{\mathbf{p}_T^2 + M_b^{*2}}}{E_b^*(\mathbf{p})} \mu_b B, \quad (18)$$

and

$$u_b(\mathbf{p}, s) \bar{u}_b(\mathbf{p}, s) = \frac{1}{4E_b^*(\mathbf{p})} [E_b^*(\mathbf{p})\gamma_0 - \mathbf{p} \cdot \boldsymbol{\gamma} + M_b^*] (1 + s\gamma_5 \not{d}(\mathbf{p}))$$

$$\begin{aligned}
& + \frac{p_z \mu_b B}{4E_b^{*3}(\mathbf{p})} (\boldsymbol{\sigma} \cdot \mathbf{p} - M_b^* \gamma_5 \gamma_0) \\
& + \frac{s \mu_b B}{8E_b^*(\mathbf{p}) \sqrt{\mathbf{p}_T^2 + M_b^{*2}}} (-E_b^*(\mathbf{p}) \gamma^0 + M_b^* + p_z \gamma^3 - p_x \gamma^1 - p_y \gamma^2) \quad (19)
\end{aligned}$$

with

$$a(\mathbf{p}) \equiv (a_0, \mathbf{a}_T, a_z) = \frac{1}{\sqrt{\mathbf{p}_T^2 + M_b^{*2}}} (p_z, 0, 0, E_b^*(\mathbf{p})) \quad . \quad (20)$$

Detailed derivations of these expressions of Eq. (19) are presented in appendix A. The second and third terms of Eq. (19) do not appear in the non-relativistic framework, but their contributions are negligibly small and can be omitted in the present work.

For the electron contribution in Eq. (14), we have to use another treatment. This is because electron mass is very small, and its current is almost a Dirac current

$$\mathcal{L}_{eM} = -e \bar{\psi}_e \gamma_\mu \psi_e A^\mu, \quad (21)$$

where  $\psi_e$  is the electron field. Also, the effect of a strong magnetic field on electrons may not be a small perturbation. The electron energy in the presence of a strong magnetic field is generally given by

$$e_e(n, k_z; s) = \sqrt{k_z^2 + m_e^2 + eB(2n + 1 - s)}, \quad (22)$$

where  $n$  stands for the Landau levels of the electrons.

But the electron wave function also becomes a plane wave in the limit of  $B \rightarrow 0$ , so that we can use the same expression as Eq. (19) for electrons, aside from the spin vector. The upper component of the electron Dirac spinor is an eigenvector of the matrix  $\sigma_z$ . The spin vector in the rest frame of the electron is then  $(0; 0, 0, 1)$ . In the matter frame the boosted spin vector can be written as

$$a(\mathbf{k}) = a_e(\mathbf{k}) \equiv \left( \frac{k_z}{m_e}, \frac{k_z \mathbf{k}_T}{m_e(E_e(\mathbf{k}) + m_e)}, 1 + \frac{k_z^2}{m_e(E_e(\mathbf{k}) + m_e)} \right) \quad , \quad (23)$$

where  $k_z$  and  $\mathbf{k}_T$  are the components along the  $z$ -direction and perpendicular to the  $z$ -direction, respectively.

When  $\sqrt{2eB} \ll \varepsilon_e$ , the summation over  $n$  can be approximated as an integration over energy, i.e.

$$\sum_n \rightarrow \frac{1}{2eB} \int dx_T \quad , \quad (x_T = 2eB(n + \frac{1}{2})) \quad . \quad (24)$$

Note that the variable  $x_T$  corresponds to  $\mathbf{k}_T^2$  in the limit of  $B \rightarrow 0$ . Then, the expectation value of an operator  $\hat{\mathcal{O}}$  is given by

$$\begin{aligned} \langle \hat{\mathcal{O}} \rangle &= \frac{2eB}{(2\pi)^2} \sum_s \sum_n \int dk_z n_e(e_e(n, k_z, s)) \mathcal{O}(n, k_z, s) \\ &\approx \frac{1}{(2\pi)^2} \sum_s \int dx_T \int dk_z n_e(e_e(x_T, k_z, s)) \mathcal{O}(x_T, k_z, s) \\ &\approx \frac{1}{(2\pi)^3} \sum_s \int d^3k n_e(e_e(\mathbf{k}, s)) \mathcal{O}(\mathbf{k}, s), \end{aligned} \quad (25)$$

where the electron energy is approximately given as  $e_e = \sqrt{\mathbf{k}^2 + m_e^2} - eBs$ .

Actual calculations are performed in the limit of  $m_e \rightarrow 0$ , so that the electron energy and the spin vector are approximated by

$$e_e \approx \sqrt{\mathbf{k}^2 + m_e^2} - \frac{eBs}{2\sqrt{\mathbf{k}^2 + m_e^2}} \approx |\mathbf{k}| + \frac{m_e}{|\mathbf{k}|} \mu_e Bs, \quad (26)$$

$$a_e(\mathbf{k}) \approx \frac{1}{m_e} \left( k_z, \frac{k_z \mathbf{k}_T}{|\mathbf{k}|}, \frac{k_z^2}{|\mathbf{k}|} \right), \quad (27)$$

where  $\mu_e = -e/2m_e$ .

As already commented at the end of Sec. III, the fractions of the anti-leptons and anti-baryons are negligibly small, and these particles do not contribute to the neutrino reactions. Therefore, we ignore the contributions from antiparticles, and omit the superscript '+' in the single particle energies  $e_b^{(\pm)}(\mathbf{p})$  and the Fermi distribution  $n_b^{(\pm)}(\mathbf{p}, s)$ .

## B. Neutrino Reaction Cross-Sections

In this subsection we consider neutrino reactions in NS matter consisting of electrons and baryons (i.e. protons, neutrons and  $\Lambda$ s). The weak interaction part of the Lagrangian density  $\mathcal{L}_W$  in Eq. (1) is written as

$$\mathcal{L}_W = \frac{G_F}{2} \left\{ \sum_{\alpha, \beta} \bar{\psi}_\alpha \gamma_\mu (c_V - c_A \gamma_5) \psi_\beta \right\}^2, \quad (28)$$

where the indices  $\alpha$  and  $\beta$  indicate particles comprising the NS matter. The  $c_V$  and  $c_A$  are the weak vector and axial coupling constants dependent on each channel.

We utilize the impulse approximation, *i.e.* individual collisions between the initial neutrino and the constituent particles. We consider both neutrino scattering ( $\nu_e \rightarrow \nu'_e$ ) channels

$$\nu_e + p \rightarrow \nu'_e + p', \quad (29)$$

$$\nu_e + n \rightarrow \nu'_e + n', \quad (30)$$

$$\nu_e + \Lambda \rightarrow \nu'_e + \Lambda', \quad (31)$$

$$\nu_e + e^- \rightarrow \nu'_e + e'^-, \quad (32)$$

and absorption ( $\nu_e \rightarrow e^-$ ) channels

$$\nu_e + n \rightarrow e^- + p, \quad (33)$$

$$\nu_e + \Lambda \rightarrow e^- + p. \quad (34)$$

As noted above, we consider rather low temperatures,  $T \ll \varepsilon_b$ . Therefore, we may ignore the contribution from antiparticles. In addition, we treat this system as partially spin-polarized owing to the magnetic field. The cross-section can then be described in terms of the initial and final lepton momenta  $\mathbf{k}_i$  and  $\mathbf{k}_f$

$$\begin{aligned} \frac{d^3\sigma}{dk_f^3} &= \frac{G_F^2}{16\pi^2} V \sum_{\alpha,\beta} \sum_{s_l, s_i, s_f} [1 - n_l(e_l(\mathbf{k}_f, s_l))] \int \frac{d^3p_i}{(2\pi)^3} \frac{d^3p_f}{(2\pi)^3} W_{BL}(k_i, k_f, p_i, p_f; \alpha, \beta) \\ &\quad \times n_\alpha(e_\alpha(\mathbf{p}_i, s_i)) [1 - n_\beta(e_\beta(\mathbf{p}_f, s_f))] \\ &\quad \times (2\pi)^4 \delta^3(\mathbf{k}_i + \mathbf{p}_i - \mathbf{k}_f - \mathbf{p}_f) \delta(|\mathbf{k}_i| + e_\alpha(\mathbf{p}_i) - e_\beta(\mathbf{p}_f) - e_l(\mathbf{k}_f)), \end{aligned} \quad (35)$$

where  $V$  is the volume of the system, and index  $l$  denotes final lepton species. Indices  $\alpha$  and  $\beta$  denote initial and final baryons and electrons, which have momenta  $p_i$  and  $p_f$ , respectively. The function  $W_{BL}$  in Eq. (35) is defined as a product of lepton and hadron weak currents

$$W_{BL} = \frac{1}{4|\mathbf{k}_i||\mathbf{k}_f|E_\alpha^*(\mathbf{p}_i)E_\beta^*(\mathbf{p}_f)} L^{\mu\nu} N_{\mu\nu} \quad (36)$$

with

$$L^{\mu\nu} = \frac{1}{4} \text{Tr} \{ (\not{k}_f + m_l)(1 + \gamma_5 \not{d}_l s_l) \gamma^\mu (1 - \gamma_5) \not{k}_\alpha \gamma^\nu (1 - \gamma_5) \}, \quad (37)$$

and

$$\begin{aligned} N_{\mu\nu} &= \frac{1}{4} \text{Tr} \{ (\not{p}_f + M_\beta^*)(1 + \gamma_5 \not{d}_\beta s_f) \gamma_\mu (c_V - c_A \gamma_5) \\ &\quad \times (\not{p}_i + M_\alpha^*)(1 + \gamma_5 \not{d}_\alpha s_i) \gamma_\nu (c_V - c_A \gamma_5) \}, \end{aligned} \quad (38)$$

where  $m_l$  is the mass of the final lepton.

Since we take the weak magnetic field limit, we treat this system as partially spin-polarized owing to the magnetic field. Then the Fermi distribution and the delta function

in the above equations can be expanded in terms of the magnetic field  $B$ . Finally, the cross-section can be summarized as a sum of two contributions,  $\sigma_{S,A}^0$  independent of  $B$  and  $\Delta\sigma_{S,A}$  depending on  $B$ ,

$$\frac{d^3\sigma_{S,A}}{dk_f^3} = \frac{d^3\sigma_{S,A}^0}{dk_f^3} + \frac{d^3\Delta\sigma_{S,A}}{dk_f^3}, \quad (39)$$

where the indices  $S$  and  $A$  indicate the cross-sections for scattering or absorption, respectively.

For the absorption process, we use the energy delta function in Eq. (35) to further separate the magnetic part of the cross-section of Eq. (39) into two parts

$$\Delta\sigma_A = \Delta\sigma_M + \Delta\sigma_{el}, \quad (40)$$

where first and second terms are the contribution from target particle and outgoing electron, which appear only in the absorption ( $\nu_e \rightarrow e^-$ ) process. Detailed derivations are written in the appendix B.

The first term of Eq. (40),  $\Delta\sigma_M$ , is calculated as

$$\frac{d^2\Delta\sigma_M}{dk_f d\Omega_f} = \frac{4\pi G_F^2 B}{(2\pi)^6} \frac{|\mathbf{k}_f|}{|\mathbf{k}_i|} (1 - n_l(|\mathbf{k}_f|)) \sum_{\alpha,\beta} (T_A + T_B) \quad , \quad (41)$$

where

$$\begin{aligned} T_A &= \frac{1}{|\mathbf{q}|} \int \frac{d^3p_i}{|\mathbf{p}_i| E_\alpha^*} \delta(t - t_p) \left\{ n'_\alpha(E_\alpha^* + U_0(\alpha)) [1 - n_\beta(E_\beta^* + U_0(\beta))] \mu_\alpha \tilde{W}_i \right. \\ &\quad \left. + n'_\beta(E_\beta^* + U_0(\beta)) n_\alpha(E_\alpha^* + U_0(\alpha)) (\mu_\alpha \tilde{W}_i - 2\mu_\beta \tilde{W}_f) \right\}, \\ T_B &= -\frac{1}{\mathbf{q}^2} \int \frac{d^3p_i}{\mathbf{p}_i^2 E_\alpha^*} (E_\alpha^* + q_0) \delta(t - t_p) n_\alpha(E_\alpha^* + U_0(\alpha)) \\ &\quad \times [1 - n_\beta(E_\beta^* + U_0(\beta))] \left( \mu_\alpha \frac{\partial \tilde{W}_i}{\partial t} - \mu_\beta \frac{\partial \tilde{W}_f}{\partial t} \right) \quad , \end{aligned} \quad (42)$$

with

$$\begin{aligned} \tilde{W}_i &= c_V^2 \{ [k_f \cdot (M_\beta^* p_i - M_i^* p_f)] (k_i \cdot b_\alpha) - [k_i \cdot (M_\beta^* p_i - M_\alpha^* p_f)] (k_f \cdot b_\alpha) \} \\ &\quad + c_A^2 \{ [-k_f \cdot (M_\beta^* p_i + M_\alpha^* p_f)] (k_i \cdot b_\alpha) + [k_i \cdot (M_\beta^* p_i + M_\alpha^* p_f)] (k_f \cdot b_\alpha) \} \\ &\quad - 2c_V c_A M_\alpha^* \{ (k_f \cdot p_f) (k_i \cdot b_\alpha) + (k_i \cdot p_f) (k_f \cdot b_\alpha) \}, \end{aligned} \quad (43)$$

$$\begin{aligned} \tilde{W}_f &= c_V^2 \{ [k_f \cdot (M_\beta^* p_i - M_\alpha^* p_f)] (k_i \cdot b_\beta) - [k_i \cdot (M_\beta^* p_i - M_\alpha^* p_f)] (k_f \cdot b_\beta) \} \\ &\quad + c_A^2 \{ [k_f \cdot (M_\beta^* p_i + M_\alpha^* p_f)] (k_i \cdot b_\beta) - [k_i \cdot (M_\beta^* p_i + M_\alpha^* p_f)] (k_f \cdot b_\beta) \} \\ &\quad - 2c_V c_A M_\beta^* \{ (k_i \cdot p_i) (k_f \cdot b_\beta) + (k_f \cdot p_i) (k_i \cdot b_\beta) \} \end{aligned} \quad (44)$$

and

$$b_\alpha = \frac{\sqrt{\mathbf{p}_T^2 + M_\alpha^{*2}}}{E_\alpha^*(\mathbf{p})} a_\alpha(p_\alpha) . \quad (45)$$

In these equations the four momenta  $p_i$  and  $p_f$  are defined by  $p_i \equiv (E_\alpha^*(\mathbf{p}_i), \mathbf{p}_i)$  and  $p_f \equiv (E_\beta^*(\mathbf{p}_f), \mathbf{p}_f)$ .

When the target particle is an electron, the above expression is slightly altered. When both the initial and final particles are electrons, the above equations are written as

$$\begin{aligned} \tilde{W}_i/m_e = & \delta_{\beta e} \{ c_V^2 [(k_f \cdot (p_i - p_f)) (k_i \cdot b_i) - (k_i \cdot (p_i - p_f)) (k_f \cdot b_i)] \\ & + c_A^2 [(-k_f \cdot (p_i + p_f)) (k \cdot b_\alpha) + (k_i \cdot (p_i + p_f)) (k_f \cdot b_\alpha)] \\ & - 2c_V c_A [(k_f \cdot p_f)(k_i \cdot b_\alpha) + (k_f \cdot b_\alpha)(k_i \cdot p_f)] \} , \end{aligned} \quad (46)$$

$$\begin{aligned} \tilde{W}_f/m_e = & \delta_{\alpha e} \{ c_V^2 [(k_f \cdot (p_i - p_f)) (k_i \cdot b_\beta) - (k_i \cdot (p_i - p_f)) (k_f \cdot b_\beta)] \\ & + c_A^2 [[k_f \cdot (p_i + p_f)] (k_i \cdot b_\beta) - [k_i \cdot (p_i + p_f)] (k_f \cdot b_\beta)] \\ & - 2c_V c_A [(k_i \cdot p_i)(k_f \cdot b_\beta) + (k_f \cdot p_i)(k_i \cdot b_\beta)] \} , \end{aligned} \quad (47)$$

and

$$b_{i,f} = b_e(k_f) = \frac{m_e}{|\mathbf{p}_{i,f}|} a_e(p_{i,f}) . \quad (48)$$

In the actual calculation we take the limit of  $m_e \rightarrow 0$ , keeping  $\mu_e \tilde{W}_{i,f}$  and  $b_{i,f}$  finite.

The second term in Eq. (40),  $\Delta\sigma_{el}$ , is calculated as

$$\begin{aligned} & \left[ \frac{G_F^2 B}{16\pi^5 |\mathbf{q}| |\mathbf{k}_i| |\mathbf{k}_f|} \right]^{-1} \frac{d^3}{dk_f^3} \Delta\sigma_{el} \\ & \approx \sum_{\alpha,\beta} n'_i(|\mathbf{k}_f|) \int \frac{d^3 p_i}{|\mathbf{p}_i| E_\alpha^* E_\beta^*} \delta(t - t_p) (E_\alpha^* + \omega) n_\alpha(E_\alpha^* + U_0(\alpha)) [1 - n_\beta(E_\beta^* + U_0(\beta))] \tilde{W}_e \\ & + \sum_{\alpha,\beta} [1 - n_i(|\mathbf{k}_f|)] \int \frac{d^3 p_i}{|\mathbf{p}_i| E_\alpha^*} \delta(t - t_p) n_\alpha(E_\alpha^* + U_0(\alpha)) n'_\beta(E_\beta^* + U_0(\beta)) \tilde{W}_e \\ & - \sum_{\alpha,\beta} [1 - n_i(|\mathbf{k}_f|)] \int \frac{d^3 p_i}{\mathbf{p}_i^2 E_\alpha^*} \delta(t - t_p) (E_\alpha^* + \omega) n_\alpha(E_\alpha^* + U_0(\alpha)) \\ & \quad \times [1 - n_\beta(E_\beta^* + U_0(\beta))] \frac{\partial \tilde{W}_e}{\partial t} \end{aligned} \quad (49)$$

with

$$\begin{aligned} \tilde{W}_e & = \frac{m_e \mu_e}{|\mathbf{k}_f|} W_e \\ & = -c_V^2 [(k_i \cdot p_f)(p_i \cdot b_e) + (k_i \cdot p_i)(p_f \cdot b_e) - M_\beta M_\alpha (k_i \cdot b_e)] \end{aligned}$$

$$\begin{aligned}
& -c_A^2 [(k_i \cdot p_f)(p_i \cdot b_e) + (k_i \cdot p_i)(p_f \cdot b_e) + M_\beta M_\alpha (k_i \cdot b_e)] \\
& + 2c_V c_A [(k_i \cdot p_f)(p_i \cdot b_e) - (k_i \cdot p_i)(p_f \cdot b_e)] \quad , \quad (50)
\end{aligned}$$

where  $b_e = m_e a_e(k_f)/|\mathbf{k}_f|$ .

### C. Non-Relativistic Limit

In order to clarify relativistic effects we take the non-relativistic limit,  $p_\alpha = (M_\alpha; 0)$ ,  $p_f = (M_\beta; 0)$ ,  $a_\alpha = (0, 0, 0, 1)$ . Then the cross-sections become

$$\frac{d^2 \sigma_0}{dk_f d\Omega_f} = \frac{G_F^2}{16\pi^5} [1 - n_l(|\mathbf{k}_f|)] \mathbf{k}_f^2 \left[ (c_V^2 + 3c_A^2) + (c_V^2 - c_A^2) \frac{\mathbf{k}_i \cdot \mathbf{k}_f}{|\mathbf{k}_i||\mathbf{k}_f|} \right] R_1 \quad , \quad (51)$$

$$\begin{aligned}
\frac{d^2 \Delta \sigma_M}{dk_f d\Omega_f} &= \frac{G_F^2}{16\pi^5} B [1 - n_l(|\mathbf{k}_f|)] \mathbf{k}_f^2 \left\{ \cos \theta_i \sum_{\alpha, \beta} [\mu_\alpha c_A (c_V + c_A) R_2 - 2\mu_\beta c_A (c_V - c_A) R_3] \right. \\
&\quad \left. + \sum_{\alpha, \beta} \cos \theta_f [\mu_\alpha c_A (c_V - c_A) R_2 + 2\mu_\beta c_A (c_V + c_A) R_3] \right\} \quad (52)
\end{aligned}$$

with

$$R_1 = \int d^3 p \delta(|\mathbf{k}_i| - |\mathbf{k}_f| + E_\alpha(\mathbf{p}) - E_\beta(\mathbf{p} + \mathbf{q})) n_\alpha(E_\alpha) [1 - n_\beta(E_\beta)] \quad , \quad (53)$$

$$\begin{aligned}
R_2 &= \int d^3 p \delta(|\mathbf{k}_i| - |\mathbf{k}_f| + E_\alpha(\mathbf{p}) - E_\beta(\mathbf{p} + \mathbf{q})) \\
&\quad \times \{ n'_\alpha(E_\alpha) [1 - n_\beta(E_\beta)] + n_\alpha(E_\alpha) n'_\beta(E_\beta) \} \quad , \quad (54)
\end{aligned}$$

$$R_3 = \int d^3 p \delta(|\mathbf{k}_i| - |\mathbf{k}_f| + E_\alpha(\mathbf{p}) - E_\beta(\mathbf{p} + \mathbf{q})) n_\alpha(E_\alpha) n'_\beta(E_\beta) \quad , \quad (55)$$

where  $E_\alpha$  is the single particle energy of particle  $a$ , and  $\theta_i$  and  $\theta_p$  are the polar angles of the initial and final leptons.

Lai and Qian [42] made a further approximation with the long wave length limit  $|\mathbf{k}_i| - |\mathbf{k}_f| \rightarrow 0$ , and made  $R_1$ ,  $R_2$  and  $R_3$  independent of  $\theta_i$  and  $\theta_f$ . Then,  $\sigma_M$  is a linear function of  $\theta_i$  and  $\theta_f$ . This makes it possible to solve the Boltzmann equation analytically. However, this approach does not include the effects of Fermi motion and cannot be used for the electron contribution because its mass is taken to be zero. Therefore, this approximation is only valid in the very low density regime,  $\rho_B \lesssim 0.1\rho_0$ .

## IV. RESULTS AND DISCUSSION OF NEUTRINO CROSS-SECTIONS

In this section we present the cross-sections for neutrino scattering ( $\nu_e \rightarrow \nu_e$ ) and absorption ( $\nu_e \rightarrow e^-$ ) in matter with and without a magnetic field. We set the lepton fraction to be fixed as  $Y_L = 0.4$ , and the neutrino incident energy is taken to be its chemical potential,  $|\mathbf{k}_i| = \varepsilon_\nu$ , unless otherwise noted. In Eq. (28) we utilize the parameters for the weak-interaction,  $c_V$  and  $c_A$  from Ref. [21].

### A. Neutrino Cross-Sections without a Magnetic Field

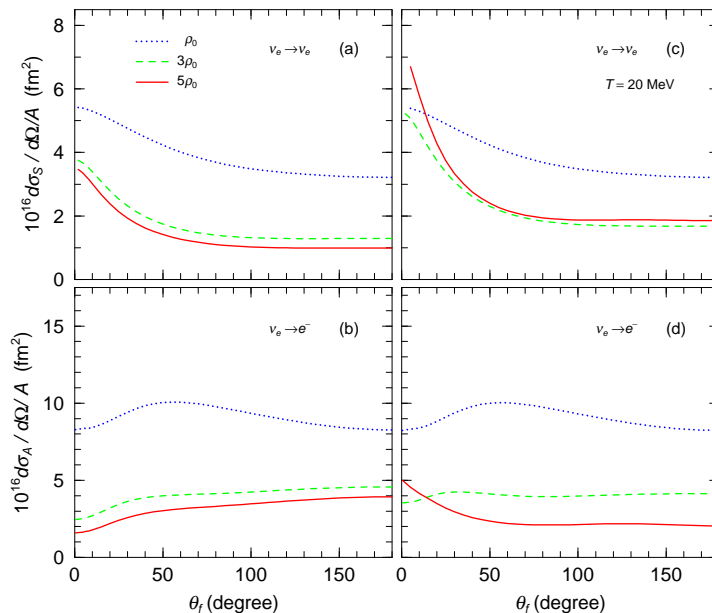


FIG. 2: (Color online) Density dependence of the scattering (a and c) and absorption differential cross-sections (b and d) of neutrinos in neutron-star matter at  $T = 20$  MeV without  $\Lambda$ s (a and b) and with  $\Lambda$ s (c and d). The initial neutrino angle is taken to be  $\theta_i = 0^\circ$ . Dotted, dashed and solid lines represent the results for  $\rho_B = \rho_0$ ,  $3\rho_0$  and  $5\rho_0$ , respectively.

In Fig. 2 we show the density dependence of the differential cross-section per baryon at  $T = 20$  MeV for the scattering (a and c) and absorption (b and d) of neutrinos in matter without  $\Lambda$ s (a and b) and with  $\Lambda$ s (c and d). The subscripts 'S' or 'A' refer to the scattering or absorption cross-sections, respectively. Solid and dashed lines show the results in matter including  $\Lambda$ s or no  $\Lambda$ s, respectively. We see that the scattering cross-sections are forward peaked, while the absorption cross-sections decrease at forward angles when  $\rho_B \leq 3\rho_0$ .



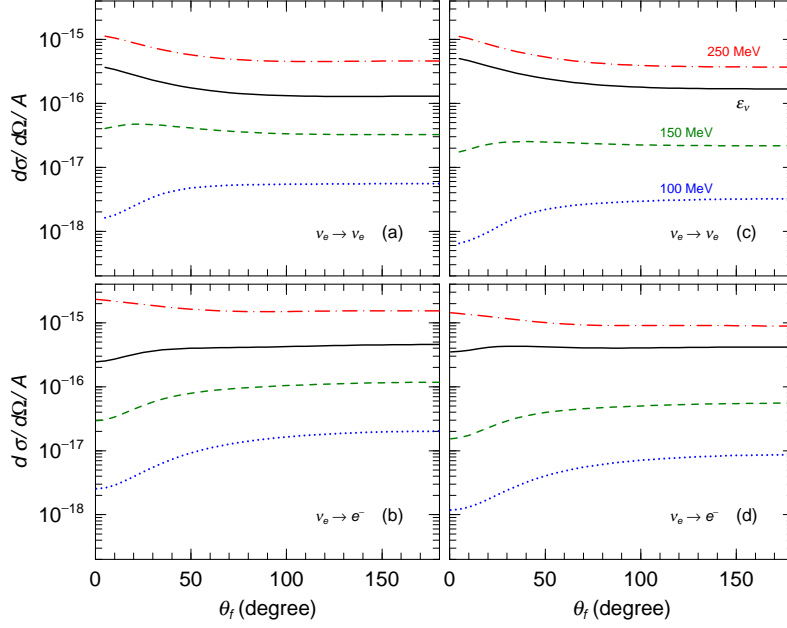


FIG. 3: (Color online) Scattering (a and c) and absorption differential cross-sections (b and d) for neutrinos for  $\theta_i = 0$  versus the final lepton angle  $\theta_f$  with various incident neutrino energies in PNS matter at  $\rho_B = 3\rho_0$  and  $T = 20$  MeV. Dotted, dashed and dot-dashed lines show the results for incident neutrino energies  $|\mathbf{k}_i| = 100, 150,$  and  $250$  MeV, respectively. Solid lines show results for the incident neutrino energy equal to the neutrino chemical potential, i.e.  $|\mathbf{k}_i| = \varepsilon_\nu$ .

In Fig. 3, we show the energy dependence of the differential cross-sections per baryon at  $\rho_B = 3\rho_0$  and  $T = 20$  MeV for various incident neutrino energies. The solid lines show the results for the incident neutrino energies equal to the neutrino chemical potentials, i.e.  $|\mathbf{k}_i| = \varepsilon_\nu$ . Dotted, dashed and dot-dashed lines represent the results at  $|\mathbf{k}_i| = 100, 150$  and  $250$  MeV, respectively.

For  $|\mathbf{k}_i| = 100$  MeV, the cross-sections show a minimum at forward angles. With the increase of incident energy, however, the cross-sections gradually become larger and finally become peaked at forward angles. This behavior arises from the the difference in Fermi distributions between the spin-up and spin-down particles, as was discussed in Ref. [44]. This Pauli blocking affects the results at all angles, and, in particular, manifests itself at forward angles. However, this Pauli blocking effect becomes smaller at higher incident energies as shown in Fig. 3. We have confirmed that the cross-sections always show forward peaks when we turn off the Pauli blocking term for the final lepton,  $(1 - n_l)$ . We can therefore conclude that the Pauli blocking effect is clearly exhibited at low incident energy

as a suppression of the differential cross-sections at forward angles.

## B. Differential Neutrino Cross-Sections in a Magnetic Field

In this subsection we discuss effects of a magnetic field on the neutrino reactions in neutron-star matter. For illustration, we first calculate the differential cross-sections per baryon,  $d\sigma_{S,A}/d\Omega/A$  with an initial neutrino angle of  $\theta_i = 0^\circ$  at a matter density of  $\rho_B = 3\rho_0$  and a magnetic field of  $B = 2 \times 10^{17}\text{G}$ . This gives  $\mu_N B = 0.63\text{ MeV}$ , where  $\mu_N$  is the nuclear magneton. The initial momenta are taken to be equal to the chemical potential in each case, *i.e.*  $|\mathbf{k}_i| = \varepsilon_\nu$ .

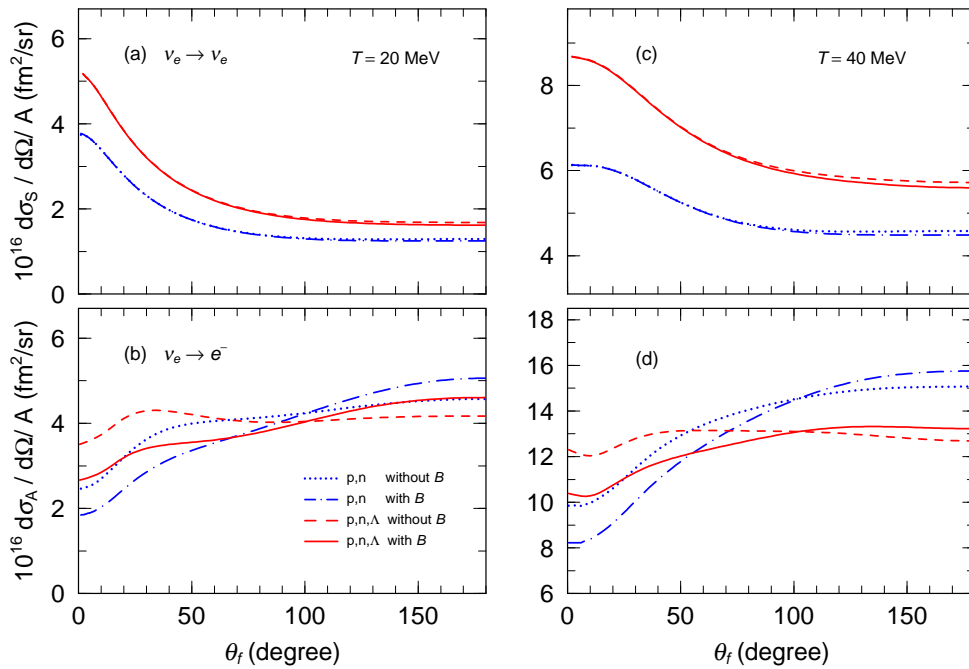


FIG. 4: (Color online) Effects of magnetic fields on the differential cross sections per baryon  $d\sigma/d\Omega/A$ , from Eq. (39) in units of  $10^{-16}\text{ fm}^2$ . This figure is obtained at a density of  $\rho_B = 3\rho_0$  at  $T = 20\text{ MeV}$  (a and b) and  $40\text{ MeV}$  (c and d). Upper (lower) panels are for neutrino scattering (absorption). Initial momentum and angle of incident neutrinos are taken to be  $|\mathbf{k}_i| = \varepsilon_\nu$  and  $\theta_i = 0^\circ$ . Solid and short-dashed lines represent results including  $\Lambda$ s with and without a magnetic field  $B = 2 \times 10^{17}\text{G}$ , respectively. Dot-dashed and dotted lines represent results without  $\Lambda$ s.

In Fig. 4 we show the neutrino scattering ( $\nu_e \rightarrow \nu_e$ ) cross-sections in the upper panels (a and c) and the absorption ( $\nu_e \rightarrow e^-$ ) cross-sections in lower panels (b and d), in Eq. (39). Left and right panels are for temperatures  $T = 20$  and  $40\text{ MeV}$ , respectively. Solid and dashed

lines show the results with and w/o  $\Lambda$ s, respectively. For reference, we also plot results without a magnetic field for both cases, and including (dot-dashed lines) and excluding (dotted lines)  $\Lambda$ s.

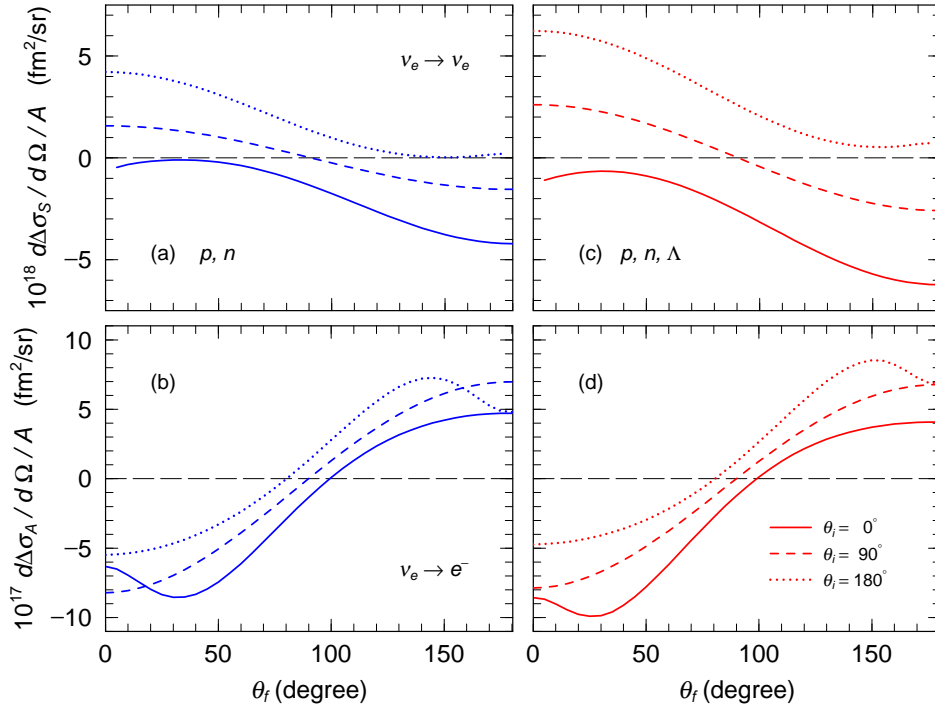


FIG. 5: (Color online) Magnetic parts of the differential cross-sections per baryon,  $d\Delta\sigma/d\Omega/A$ , corresponding to the 2nd term in Eq. (39), in units of  $10^{-16}$  fm<sup>2</sup> for neutrino scattering ( $\nu_e \rightarrow \nu_e$ ) at  $\rho_B = 3\rho_0$  for  $T = 20$  MeV without  $\Lambda$ s (a) and with  $\Lambda$ s (c). Lower panels (b and d) are the same as the upper panels but for neutrino absorption ( $\nu_e \rightarrow e^-$ ) in a system without (b) and with  $\Lambda$ s (d). Initial momentum and angle of the incident neutrinos are taken to be  $|\mathbf{k}_i| = \varepsilon_\nu$ . Solid, dashed and dotted lines represent results for  $\theta_i = 0^\circ$ ,  $90^\circ$  and  $180^\circ$ , respectively.

This figure beautifully indicates that the magnetic field does not much affect the scattering cross-sections when  $B \approx 2 \times 10^{17}$  G. Actually the contributions from each individual particle such as protons and neutrons are not so small. These contributions, however, tend to cancel each other out. However, the magnetic field suppresses the absorption cross-section in the forward direction and enhances it in the backward direction. In particular, near  $\theta_f \approx 0^\circ$ , the suppression from the magnetic field is as much as 20–30%. This contribution is almost as large as that from the  $\Lambda$  particles.

In Fig. 5 we show the magnetic parts of the differential cross-sections,  $\Delta\sigma$  of Eq. (39), at  $\rho_B = 3\rho_0$  and  $T = 20$  MeV. Upper panels are for neutrino scattering ( $\nu_e \rightarrow \nu_e$ ) and lower

panels (b and d) are for absorption ( $\nu_e \rightarrow e^-$ ). Right and left panels are for matter including and excluding  $\Lambda$ s, respectively. Solid, dashed and dotted lines represent results for incident angles, of  $\theta_i = 0^\circ$ ,  $90^\circ$  and  $180^\circ$ , respectively. In these calculations we keep the difference of the azimuthal angle between the initial and final leptons equal to zero, i.e.  $\phi_f - \phi_i = 0$ .

These calculations show that the magnetic field enhances the scattering cross-sections in the direction along the magnetic field (arctic direction). For absorption an enhancement appears in the opposite direction (antarctic direction). These asymmetries of the scattering and absorption cross-sections of neutrinos by the magnetic field would lead to the coherent effect of enhancing the neutrino drift in the arctic direction while suppressing it in the antarctic direction, as will be discussed below.

### C. Angular-integrated Neutrino Cross-Sections in a Magnetic Field and The Asymmetries

In order to discuss the effects of neutrino transfer inside the PNS at subsection E, we here calculate the scattering cross-sections integrated over the momenta of the initial neutrinos

$$\begin{aligned} \sigma_S(|\mathbf{k}_f|, \theta_f) &= \sigma_S^0(|\mathbf{k}_f|, \theta_f) + \Delta\sigma_S(|\mathbf{k}_f|, \theta_f) \\ &= \frac{1}{\rho_B} \int \frac{d^3 k_i}{(2\pi)^3} n_\nu(|\mathbf{k}_i|) \frac{d^3 \sigma_S^0(\mathbf{k}_i, \mathbf{k}_f)}{dk_f^3} + \frac{1}{\rho_B} \int \frac{d^3 k_i}{(2\pi)^3} n_\nu(|\mathbf{k}_i|) \frac{d^3 \Delta\sigma_S(\mathbf{k}_i, \mathbf{k}_f)}{dk_f^3} \end{aligned} \quad (56)$$

The absorption cross-sections are however integrated over the momenta of the final electrons as

$$\begin{aligned} \sigma_A(|\mathbf{k}_i|, \theta_i) &= \sigma_A^0(|\mathbf{k}_i|, \theta_i) + \Delta\sigma_A(|\mathbf{k}_i|, \theta_i) \\ &= \int d^3 k_f \frac{d^3 \sigma_A^0(\mathbf{k}_i, \mathbf{k}_f)}{dk_f^3} + \int d^3 k_f \frac{d^3 \Delta\sigma_A(\mathbf{k}_i, \mathbf{k}_f)}{dk_f^3} \end{aligned} \quad (57)$$

Note that the non-magnetic parts of the integrated cross-sections,  $\sigma_{S,A}^0$ , are also integrated the same way.

Figures 6 and 7 show  $\Delta\sigma_S/\sigma_S^0$  with  $|\mathbf{k}_i| = \varepsilon_\nu$  and  $\Delta\sigma_A/\sigma_A^0$  with  $|\mathbf{k}_f| = \varepsilon_\nu$  as functions of  $\theta_f$  and  $\theta_i$ , respectively, for matter densities,  $\rho_0 \leq \rho_B \leq 5\rho_0$ . We plot results for matter without  $\Lambda$ s (upper panels) and with  $\Lambda$ s (lower panels) at  $T = 20$  MeV (left panels) and  $T = 40$  MeV (right panels). Similar to the differential cross-sections, the magnetic field enhances the integrated scattering cross-sections and suppresses the integrated absorption cross-sections in the arctic direction parallel to the magnetic field  $\mathbf{B}$ . The magnetic field

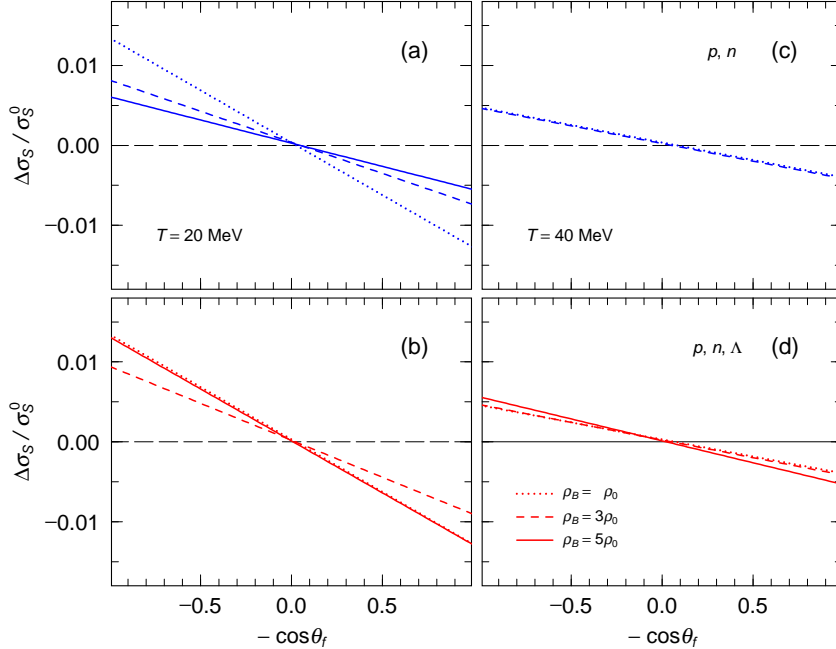


FIG. 6: (Color online) Ratios of the magnetic part of the scattering cross-sections ( $\Delta\sigma_S$ ) to the cross-sections without a magnetic-field ( $\sigma_S^0$ ) without  $\Lambda$ s (a and c) and with  $\Lambda$ s (b and d) at  $T = 20$  MeV (a and b) and at  $T = 40$  MeV (c and d). Dotted, dashed and solid lines represent the results for densities of  $\rho_B = \rho_0$ ,  $3\rho_0$  and  $5\rho_0$ , respectively.

has an opposite effect in the anti-parallel antarctic direction. Therefore, we may conclude that a magnetic field increases the neutrino emission in the arctic direction and decreases it in the antarctic direction.

In Fig. 8, we show the contribution of each constituent particle to the scattering cross-sections without  $\Lambda$ s (upper panels) and with  $\Lambda$ s (lower panels) at  $\rho_B = 3\rho_0$  (left panels) and  $\rho_B = 5\rho_0$  (right panels). Only the contribution from the protons is opposite to those from electrons, neutrons and  $\Lambda$ s because of the different signs of the magnetic moments. These contributions tend to cancel to each other, and the magnetic parts of the scattering cross-sections become slightly smaller. However, when one allows  $\Lambda$ s to appear in the system, the proton fraction decreases and in this case the cancellation is not as large as the case without  $\Lambda$ s (see Fig. 1).

Solid and dashed lines in Fig. 9 show the contributions from the  $n \rightarrow p$  and  $\Lambda \rightarrow p$  neutrino absorption processes, respectively. Upper and lower panels exhibit the results at  $\rho_B = 3\rho_0$  and  $\rho_B = 5\rho_0$ , respectively. Results in the left and right panels are divided by the non-magnetic parts of the integrated cross-sections and their respective non-magnetic

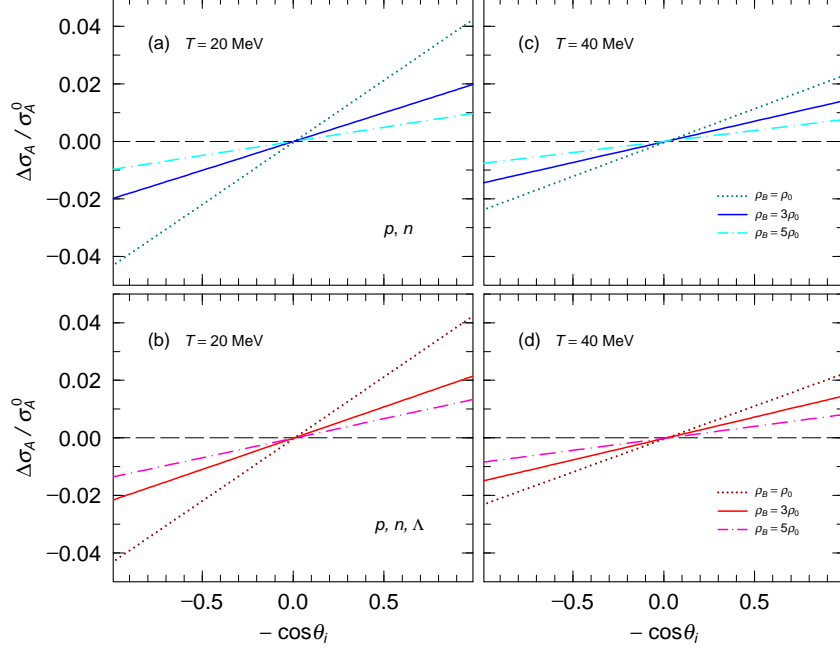


FIG. 7: (Color online) Ratios of the magnetic part of the absorption cross-sections ( $\Delta\sigma_A$ ) to the cross-sections without a magnetic-field ( $\sigma_A^0$ ) without  $\Lambda$ s (a and c) and on matter with  $\Lambda$ s (b and d) at  $T = 20$  MeV (a and b) and at  $T = 40$  MeV (c and d). Dotted, dashed and solid lines represent the results for  $\rho_B = \rho_0$ ,  $3\rho_0$  and  $5\rho_0$ , respectively.

contributions.

Contributions from the  $\Lambda \rightarrow p$  process seem to be much smaller than those from the  $n \rightarrow p$  in the left panels, but in the right panels the former contributions are as large as the latter. This apparent difference is because of the small Cabibbo angle,  $\sin^2 \theta_C \approx 5.0 \times 10^{-2}$ . Since the non-magnetic part of the  $\Lambda \rightarrow p$  process is associated with a strangeness change of  $\Delta S = 1$ , its transition probability is  $\sim \sin^2 \theta_c$  times smaller than that of the  $n \rightarrow p$ ,  $\Delta S = 0$ , process. As a result, contributions from the  $\Lambda \rightarrow p$  process to the total non-magnetic part becomes very small. However, when one divides the small contributions by the small quantities from respective non-magnetic parts, the ratio shows an interesting difference as illustrated in the right panels. With  $\Lambda$ s present, the proton fraction becomes smaller as the density changes, and the contribution from the magnetic parts of the  $\Lambda \rightarrow p$  process becomes remarkably larger.

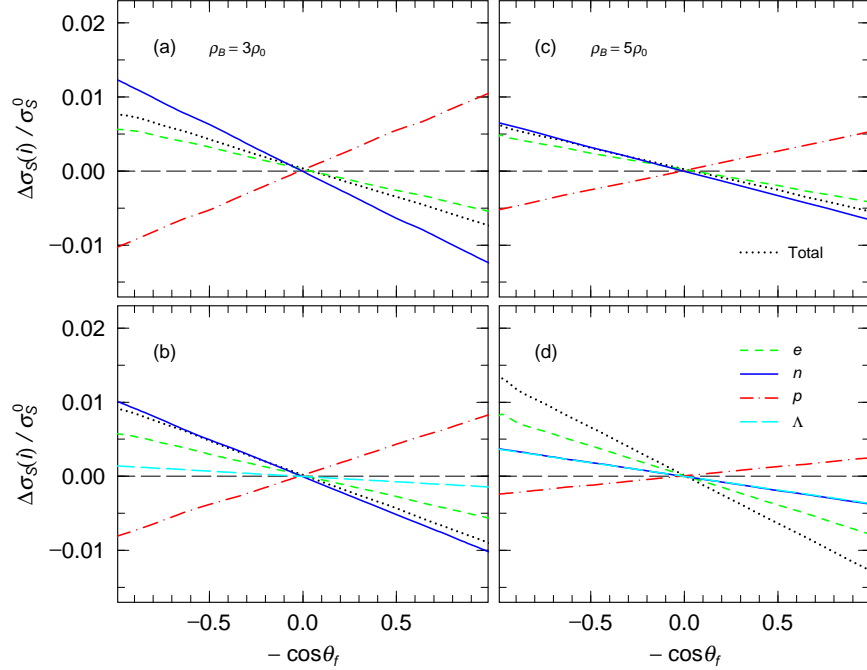


FIG. 8: (Color online) Contributions from each constituent particle to the magnetic part of the scattering cross-sections ( $\Delta\sigma_S$ ) at  $T = 20$  MeV divided by the integrated cross-sections without a magnetic-field ( $\sigma_S^0$ ). Upper(lower) panels exhibit the results without (with)  $\Lambda$ s at  $\rho_B = 3\rho_0$  (left) and  $\rho_B = 5\rho_0$  (right), respectively. Dashed, solid, dot-dashed and long dashed lines represent contributions from electrons, neutrons, protons and  $\Lambda$ s, respectively. Dotted lines represent a sum of the contributions. In panel (d), solid and long dashed lines are indiscernible.

#### D. Neutrino Mean-Free-Paths

In order to apply the above results to astronomical phenomena, we discuss the neutrino mean-free-paths (MFPs). In Fig. 10, we show the density dependence of the neutrino MFPs,  $\lambda_{S,A} = V/\sigma_{S,A}$  with the system volume  $V$ , for the scattering (a) and the absorption (c) processes at  $T = 20$  and  $40$  MeV for  $B = 0$ . For this illustration, the incident neutrino energy is fixed to be equal to its chemical potential.

The scattering and absorption MFPs rapidly decrease as the density increases up to  $\rho_B \approx (2 - 3)\rho_0$ . When the system does not include  $\Lambda$ s, both MFPs (dashed and dotted lines) decrease monotonically even beyond  $\rho_B \approx (2 - 3)\rho_0$ . When the system includes  $\Lambda$ s, the scattering MFPs also decrease, but the absorption MFPs increase in  $\rho_B \gtrsim 3\rho_0$ , because the cross-sections for  $\nu_e + \Lambda \rightarrow p + e^-$  are smaller than those of  $\nu_e + n \rightarrow p + e^-$ .

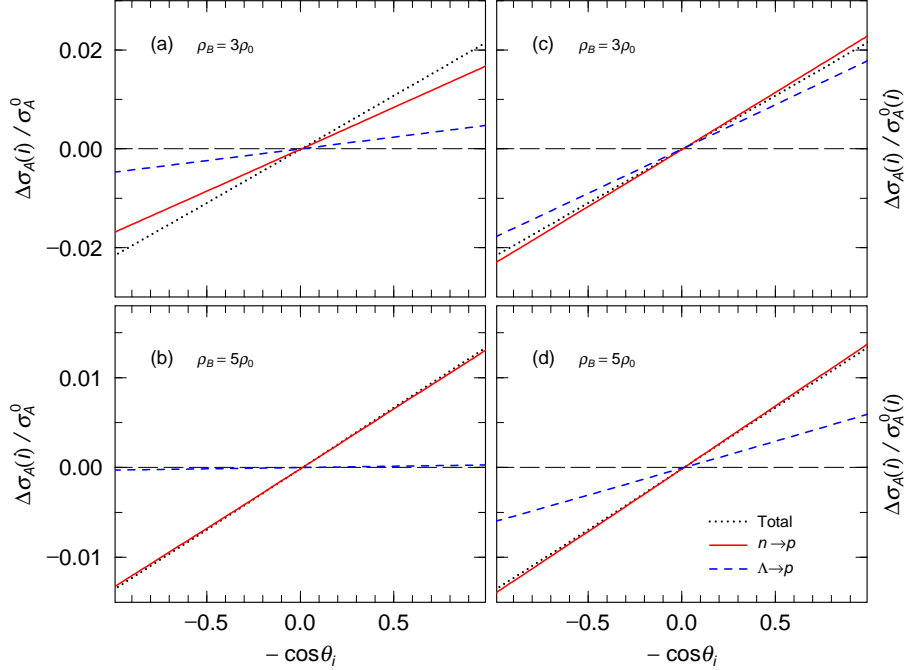


FIG. 9: (Color online) Contributions from each constituent particle in the magnetic part of the absorption cross-sections ( $\Delta\sigma_A$ ) at  $T = 20$  MeV with  $\Lambda$ s at  $\rho_B = 3\rho_0$  (upper) and  $\rho_B = 5\rho_0$  (lower panels). Left and right panels exhibit results divided by the non-magnetic parts of the total cross-sections ( $\sigma_A^0$ ) and their non-divided respective contributions ( $\sigma_A^0(i)$ ). Solid and dashed lines represent the contributions from the  $n \rightarrow p$  and  $\Lambda \rightarrow p$  processes, respectively.

In addition, we show the magnetic contributions to the MFPs,  $\Delta\lambda_{S,A} \equiv [V/\sigma(0^\circ) - V/\sigma(180^\circ)]/2$ , in the lower panels (b and d). We should note that the  $\sigma$  contribution from the scattering process is calculated by an integration over final angle, which is not the same as  $\sigma_S$  defined in Eq. (56). We see, again, that the contribution of the magnetic field is  $\sim 1 - 2\%$  of the non-magnetic parts.

The slopes of the magnetic parts of the neutrino cross-sections  $\Delta\sigma_{S,A}$  are almost constant as a function of  $\cos\theta_{i,f}$  (see Figs. 6 and 7). Hence if we define the slopes as  $S_{S,A} = (\Delta\sigma_{S,A}/\sigma_{S,A}^0)/\cos\theta_{i,f}$ , the integrated cross-sections  $\Delta\sigma_{S,A}$  can be approximately written as

$$\sigma_{S,A} \approx \sigma_{S,A}^0(1 + S_{S,A} \cos\theta_{i,f}). \quad (58)$$

The discrepancy in the use of this formula is estimated to be less than 1 %.

Since  $S_S > 0$  and  $S_A < 0$ , the neutrinos scatter and absorb in the arctic direction due to the magnetic field. In Fig. 11, we show the density dependence of  $S_S$  (a) and  $S_A$  (b). It



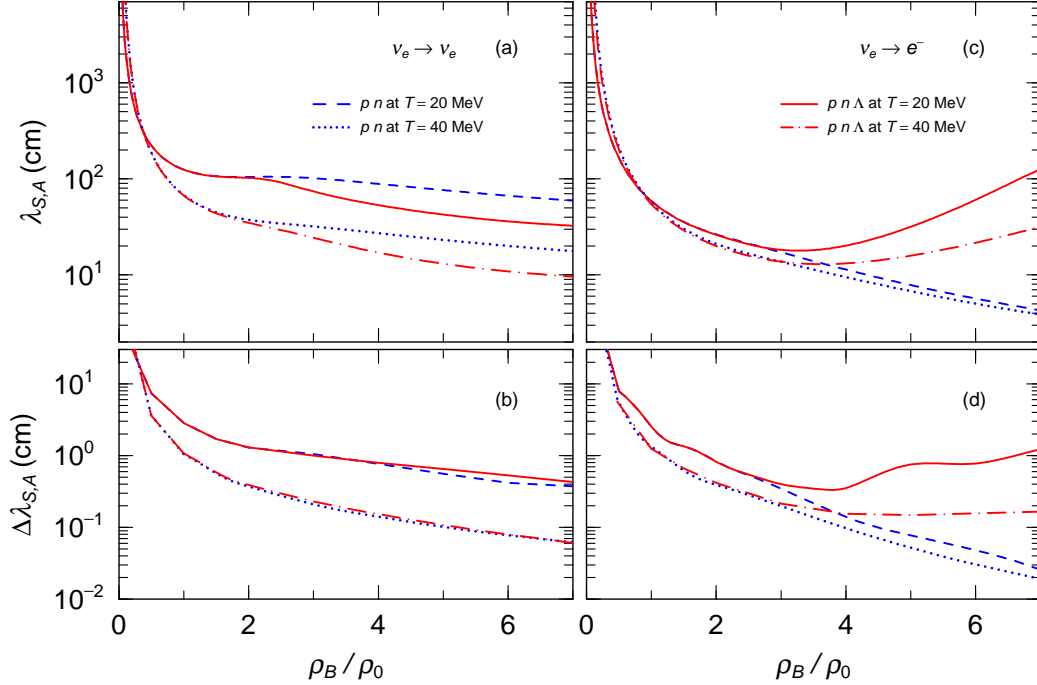


FIG. 10: (Color online) Upper panels show the neutrino MFP for scattering (a) and absorption (c) without a magnetic field. The lower panels show the magnetic contribution to the MFP for scattering (b) and absorption (d). Here the neutrino incident energy is fixed as the chemical potential. Since the magnetic part of the MFP for scattering is negative, we multiply by  $(-1)$ . Solid and dashed lines represent the results at  $T = 20$  MeV with and without  $\Lambda$ s, respectively. Dot-dashed and dotted lines represent the results at  $T = 40$  MeV with and without  $\Lambda$ s, respectively.

is evident that the effects of the magnetic field become smaller as the temperature and the density increase. This density dependence arises from the fact that  $\Delta\sigma$  is approximately proportional to the fractional area of the distorted Fermi surface caused by the magnetic field. Hence, the relative strength  $\Delta\sigma_{S,A}/\sigma_{S,A}^0$  diminishes with increasing density.

However, the density dependence of  $S_S$  including  $\Lambda$ s exhibits a local minimum around  $\rho_B \approx 3\rho_0$  and increases again in the density region,  $3\rho_0 \lesssim \rho_B \lesssim (5-6)\rho_0$ . As commented before, the Lambda fraction rapidly increases for  $\rho_B \gtrsim \rho_0$ , and its contribution enhances  $S_S$  (see Fig. 1 and Fig. 8).

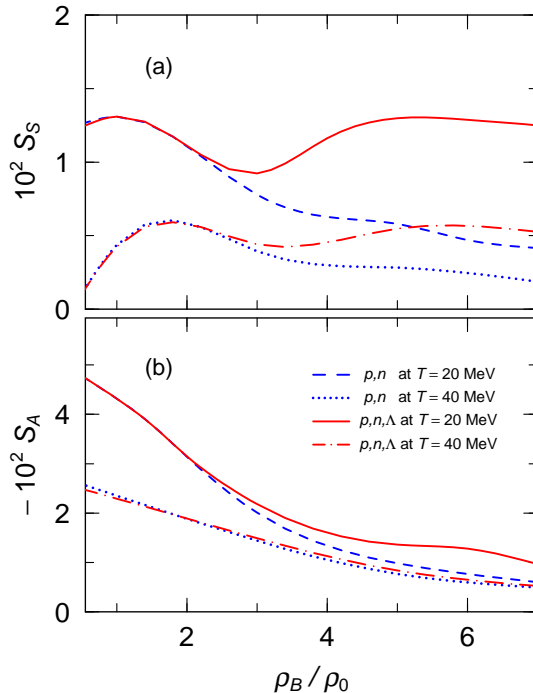


FIG. 11: (Color online) Density dependence of  $S_S$  when  $|\mathbf{k}_i| = \varepsilon_\nu$  (a) and  $S_A$  when  $|\mathbf{k}_f| = \varepsilon_\nu$  (b). Various lines show the results without  $\Lambda$ s at  $T = 20$  MeV (Dashed) and without  $\Lambda$ s at  $T = 40$  MeV (dotted), with  $\Lambda$ s at  $T = 20$  MeV (solid) and with  $\Lambda$ s at  $T = 40$  MeV (dot-dashed).

### E. Neutrino Transport and Pulsar Kick Velocities

Next we discuss implications of these findings for neutrino transport in a strongly magnetized PNS. It has been pointed out that asymmetric neutrino emissions may cause the pulsar kicks of magnetars [22, 23]. Most of the explosion energy is emitted as neutrinos. In this subsection, we estimate the momentum transfer from the asymmetric neutrino emission.

In the interpretation of actual phenomena, many different effects may contribute to the generation of pulsar kicks. One must, therefore, solve the time evolution of PNSs with a numerical simulation. However, our purpose is to examine qualitatively the effects from our asymmetric cross-sections on the kick velocity. Therefore, we can limit our discussion to only effects of the asymmetric cross-section discussed above.

For this purpose we can assume that the PNS is in local equilibrium, and that the neutrinos propagate through the dense nuclear matter in the presence of a strong magnetic field, and that eventually the neutrinos are emitted asymmetrically. Along with these assumptions, we ignore the effects of other neutrino processes, such as the direct and moderate

URCA processes [35–37], and also the momentum transfer to the medium at each local position.

The time scale for PNS evolution is much larger than that of the emitted neutrino propagating inside the PNS. Therefore, to estimate the neutrino momentum transport, we can conjecture that PNS is static, and that the neutrino transfer makes a continuous current in the equilibrium matter. Furthermore, we simplify the PNS as having a fixed temperature and magnetic field. These simplifying assumptions for the purpose of this work, which is to qualitatively examine effects of a magnetic field on the PNS momentum. Clearly, more investigation beyond the present assumptions is warranted and will be the subject of future work as discussed in Sec. VI.

### 1. Boltzmann Equation

We start with the phase-space neutrino distribution function  $f_\nu(\mathbf{r}, \mathbf{k})$  and calculate the asymmetric neutrino emission from the  $f_\nu$  function. This  $f_\nu$  satisfies the following Boltzmann equation

$$\left( \frac{\partial}{\partial t} + \hat{k} \cdot \frac{\partial}{\partial \mathbf{r}} \right) f_\nu(\mathbf{r}, \mathbf{k}) = I_{coll} \quad (59)$$

with

$$I_{coll} = \sum_{i,j} \int \frac{d^3 k_l}{(2\pi)^3} \frac{d^3 p_i}{(2\pi)^3} \frac{d^3 p_j}{(2\pi)^3} W_{if} \{ f_l(\mathbf{k}_l) f_j(\mathbf{p}_2) [1 - f_\nu(\mathbf{k})] [1 - f_i(\mathbf{p}_1)] - f_\nu(\mathbf{k}) f_i(\mathbf{p}_1) [1 - f_l(\mathbf{k}_l)] [1 - f_j(\mathbf{p}_2)] \}, \quad (60)$$

where  $W_{if}$  is the reaction probability. The index  $l$  denotes leptons, electrons or neutrinos, and the indices 1 and 2 label the target particles, e.g. baryons and electrons. In the above equations, we omit the contribution from the neutrino mean-field because its depth is about a few ten eV ( $G_F \rho_0 \approx 15$  eV), and the magnetic contribution is much less.

Here, we introduce several assumptions to obtain a solution to the Boltzmann equation. First, we assume that the system is almost in equilibrium, and that  $f_\nu(\mathbf{r}, \mathbf{k})$  can be separated into two parts

$$f_\nu(\mathbf{r}, \mathbf{k}) = f_0(\mathbf{r}, \mathbf{k}) + \Delta f(\mathbf{r}, \mathbf{k}) = \frac{1}{1 + \exp[(|\mathbf{k}| - \varepsilon_\nu(\mathbf{r}))/T]} + \Delta f(\mathbf{r}, \mathbf{k}) \quad , \quad (61)$$

where the first and the second terms are the local equilibrium part and the deviation from the equilibrium, respectively, with the neutrino chemical potential  $\varepsilon_\nu(\mathbf{r})$  at the position

$\mathbf{r}$ . The phase-space distribution functions of other particles are assumed to have local thermodynamic equilibrium distributions. In addition, we also omit the contribution from  $e^- + B \rightarrow B' + \nu_e$ . The collision term can thus be written as

$$I_{coll} \approx \sum_{ij} \int \frac{d^3k_l}{(2\pi)^3} \frac{d^3p_i}{(2\pi)^3} \frac{d^3p_j}{(2\pi)^3} \left( W_S \left\{ \Delta f(\mathbf{k}_l) [(1 - f_0(\mathbf{k}))f_i(1 - f_j) - f_0(\mathbf{k})f_i(1 - f_j)] \right. \right. \\ \left. \left. - \Delta f(\mathbf{k}) [(1 - f_0(\mathbf{k}_l))f_i(1 - f_j) - f_0(\mathbf{k}_l)f_i(1 - f_j)] \right\} \right. \\ \left. - W_A \Delta f(\mathbf{k}) [f_1(1 - f_e(\mathbf{k}_l))(1 - f_2)] \right) , \quad (62)$$

where  $W_S$  and  $W_A$  are the scattering and absorption probabilities.

We make the further assumption that only the absorption process makes a dominant contribution to the neutrino momentum transport. When the  $I_{coll}$  in Eq. (62) is integrated over  $\mathbf{k}$ , the term proportional to  $W_S$ , which represents the contribution from the scattering, becomes zero, *i.e.* this part does not change the number of emitted neutrinos. The scattering process enhances the asymmetry, but the magnetic field contribution to the scattering cross-section is small. Hence, the approximation of ignoring the scattering process may slightly underestimate the asymmetry, but does not significantly change the estimated effect.

By ignoring the scattering contributions, we can treat the neutrino trajectory as the straight line and simply express the Boltzmann equation for the neutrino transport as

$$\hat{k} \cdot \frac{\partial}{\partial \mathbf{r}} f_\nu(\mathbf{r}, \mathbf{k}) = \hat{k} \cdot \frac{\partial \varepsilon_\nu}{\partial \mathbf{r}} \frac{\partial f_0}{\partial \varepsilon_\nu} + \hat{k} \cdot \frac{\partial \Delta f}{\partial \mathbf{r}} = -\frac{\sigma_A(\mathbf{r}, \mathbf{k})}{V} \Delta f(\mathbf{r}, \mathbf{k}), \quad (63)$$

where the absorption cross-section  $\sigma_A$  is a function of  $\mathbf{k}$  and  $\rho_B(\mathbf{r})$ .

In the present approximation the neutrinos are taken to propagate along a straight line, which gives us an analytical solution for the above Boltzmann equation as explained below. First, we define a plane  $A_0$  that is perpendicular to the neutrino momentum  $\mathbf{k}$ . This plane is constructed to intersect the center of the neutron star, which we take to be the origin of the coordinate system  $\mathbf{r} \equiv (0, 0, 0)$ . Then, we introduce  $x_L$  and  $\mathbf{R}_T$  such that  $\mathbf{r} = x_L \mathbf{k} + \mathbf{R}_T$ , where  $x_L$  is the component of  $\mathbf{r}$  parallel to  $\mathbf{k}$  and  $\mathbf{R}_T \perp \mathbf{k}$ . In terms of  $x_L$  and  $\mathbf{R}_T$ , Eq. (63) can then be written as

$$\frac{\partial \varepsilon_\nu}{\partial x_L} \frac{\partial f_0}{\partial \varepsilon_\nu} + \frac{\partial \Delta f}{\partial x_L} = -\frac{\sigma_A}{V} \Delta f(x_L, \mathbf{R}_T, \mathbf{k}) , \quad (64)$$

where  $R_T \equiv |\mathbf{R}_T|$  and  $\partial \varepsilon_\nu / \partial x_L = (\hat{k} \cdot \hat{r}) \partial \varepsilon_\nu / \partial r$ . The solution is given by

$$\Delta f(x_L, \mathbf{R}_T, \mathbf{k}) = \int_0^{x_L} dy \left[ -\frac{\partial \varepsilon_\nu}{\partial y} \frac{\partial f_0}{\partial \varepsilon_\nu} \right] \exp \left[ -\int_y^{x_L} dz \frac{\sigma_A}{V} \right]. \quad (65)$$

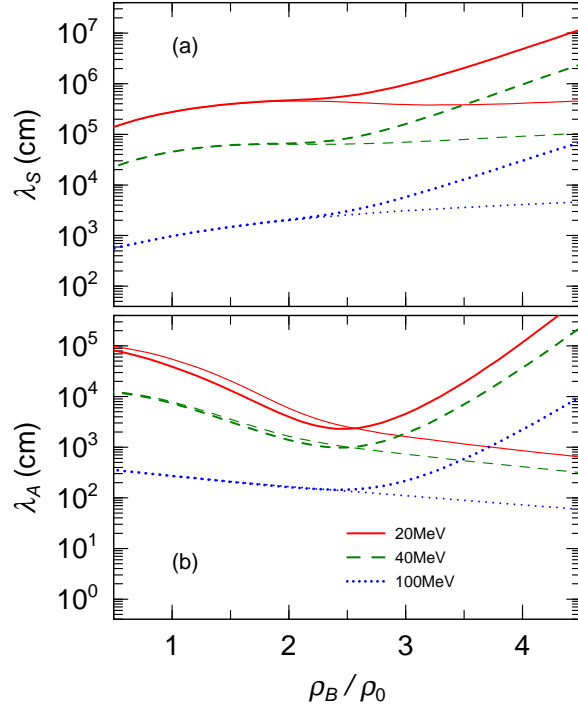


FIG. 12: (Color online) The neutrino mean-free-paths for scattering (a) absorption (b) with a neutrino energy  $E_\nu = 20$  MeV (solid line), 40 MeV (dashed line) and 100 MeV (dotted line) in neutron-star matter at  $T = 20$  MeV without a magnetic field. Thick and thin lines represent results with and without As, respectively.

As neutrinos are created inside a PNS and propagate through the matter, their intensity will be attenuated by absorption. The exponential in Eq. (65) accounts for this feature. If  $\sigma_A/V$  were sufficiently large, we would expect that very few neutrinos produced deep inside the PNS could reach the surface. That, however, is not the case.

## 2. Mean-Free-Path in NS matter

To give a more concrete picture we next analyze the mean-free path of neutrinos. Fig. 12 shows the neutrino MFPs for scattering and absorption  $\lambda_{S,A} = (\sigma_{S,A}/V)^{-1}$  for neutrino energies of  $E_\nu = 20$  MeV (solid line),  $E_\nu = 40$  MeV (dashed line), and  $E_\nu = 100$  (dotted line) in neutron-star matter at a temperature of  $T = 20$  MeV without a magnetic field.

Thick and thin lines represent the results with and without As, respectively. The MFPs for the absorption are less than a few km so that most of the neutrinos produced in the

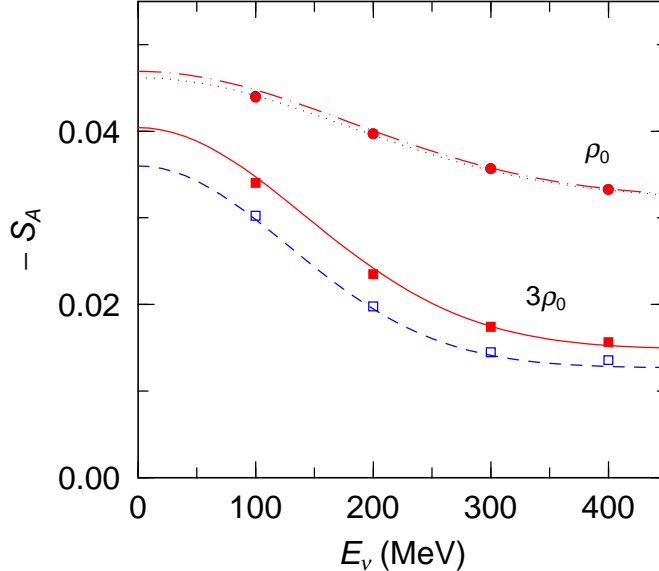


FIG. 13: (Color online) The magnetic slope parameter Eq. (67) of the neutrino absorption versus incident energy at  $T = 20$  MeV. Open and full circles show the results in the present calculation at  $\rho_B = \rho_0$  without and with  $\Lambda_s$ , respectively. Open and full squares indicate those at  $\rho_B = 3\rho_0$  without and with  $\Lambda_s$ . Dotted, dot-dashed, dashed and solid lines show results of the fitting function at  $\rho_B = \rho_0$  without and with  $\Lambda_s$ , and those at  $\rho_B = e\rho_0$  without and with  $\Lambda_s$ , respectively.

central region are absorbed. However, the neutrinos produced at the surface contribute to the net emission of neutrinos; this fact is qualitatively the same as the result obtained in Ref. [41]. In addition, we see that the neutrino MFP is longer when its energy is large because of the Pauli blocking of the final electron. As a result lower energy neutrinos are absorbed more efficiently.

Furthermore, we should note that  $\lambda_A \gg \lambda_s$  above nuclear matter density  $\rho_B \gtrsim \rho_0$ . This highlights the fact that the absorption rate is much larger than the scattering rate. This is consistent to our approximation of ignoring the scattering process.

In order to solve Eq. (65), we need to know  $\sigma_A/V$  as a function of the density  $\rho$ , the magnetic field  $B$ , the initial neutrino energy  $E_\nu$ , and the angle between the magnetic field and the initial neutrino momentum,  $\theta_\nu$ . For this calculation we have made a data base of  $\sigma_A^0$  as a function of the baryon density  $\rho_B$  and the incident neutrino energy  $E_\nu$ .

However, it is not easy to make a data base of the magnetic part of  $\Delta\sigma_M$  because it is a function of  $\rho_B$ ,  $E_\nu$  and  $\theta_\nu$  as well as  $B$ . This leads to a computationally intensive five dimensional integration. Therefore, we introduce a fitting function for the magnetic part

deduced as follows.

TABLE I: Parameters of Eqs. (67) – (70) fitted to theoretical results in Fig. 13

	$p, n$	$p, n, \Lambda$
$\mathcal{A}_0$	$7.28 \times 10^{-2}$	$6.43 \times 10^{-2}$
$\mathcal{A}_1$	$4.07 \times 10^{-2}$	$-3.22 \times 10^{-2}$
$\gamma$	0.355	0.392
$\mathcal{B}_0$	$2.96 \times 10^{-3}$	$-2.62 \times 10^{-3}$
$\mathcal{B}_1$	$7.21 \times 10^{-3}$	$2.36 \times 10^{-2}$
$\mathcal{B}_2$	$5.94 \times 10^{-3}$	$-7.01 \times 10^{-3}$
$\mathcal{B}_3$	$-2.02 \times 10^{-7}$	$7.544 \times 10^{-4}$
$\mathcal{C}_0$ (MeV <sup>2</sup> )	$1.16 \times 10^{-5}$	$-1.05 \times 10^{-5}$
$\mathcal{C}_1$ (MeV <sup>2</sup> )	$2.29 \times 10^{-7}$	$-2.57 \times 10^{-6}$
$\mathcal{C}_2$ (MeV <sup>2</sup> )	$-5.62 \times 10^{-6}$	$-3.35 \times 10^{-6}$
$\mathcal{C}_3$ (MeV <sup>2</sup> )	$1.14 \times 10^{-6}$	$8.61 \times 10^{-7}$

From Eq. (58), the angular dependence can be approximately written as

$$\sigma_A = \sigma_A^0(1 + S_A \cos \theta_\nu), \quad (66)$$

where,  $S_A$  obeys the following approximate function:

$$-S_A = \mathcal{A}_M + \mathcal{B}_M e^{-\mathcal{C}_M E_\nu^2} \quad (67)$$

with

$$\mathcal{A}_M = \mathcal{A}_0 + \mathcal{A}_1 \left( \frac{\rho_B}{\rho_0} \right)^\gamma, \quad (68)$$

$$\mathcal{B}_M = \mathcal{B}_0 + \mathcal{B}_1 \left( \frac{\rho_B}{\rho_0} \right) + \mathcal{B}_2 \left( \frac{\rho_B}{\rho_0} \right)^2 + \mathcal{B}_3 \left( \frac{\rho_B}{\rho_0} \right)^3, \quad (69)$$

$$\mathcal{C}_M = \mathcal{C}_0 + \mathcal{C}_1 \left( \frac{\rho_B}{\rho_0} \right) + \mathcal{C}_2 \left( \frac{\rho_B}{\rho_0} \right)^2 + \mathcal{C}_3 \left( \frac{\rho_B}{\rho_0} \right)^3. \quad (70)$$

All quantities except  $\rho_B$  and  $E_\nu$  are constant and adjusted to reproduce the theoretical results shown in Fig. 13 as described in the figure caption.

### 3. Proto Neutron-Star Model

To estimate the kick velocity in our model, we need baryon density profiles of PNS. Here, we assume an isothermal PNS mode which is easily calculated and effective for our purpose in this work. Baryon density profiles of our PNS model at  $T = 20$  MeV are shown in Fig. 14. We choose 20 MeV as a reasonable average isothermal approximation to a PNS. Even though the core temperature could be much more and the temperature at the neutrino sphere much less, 20 MeV is a reasonable average temperature encountered by neutrinos as they transport from the core to the neutrino-sphere.

For this illustration, we fix total gravitational mass of the PNS to be  $1.68 M_\odot$ . The appearance of  $\Lambda$  particles when  $\rho_B \gtrsim 2\rho_0$  softens the EOS. This increases the baryon density and the neutrino chemical potential. The density profiles with  $\Lambda$ s are sensitive to the temperature.

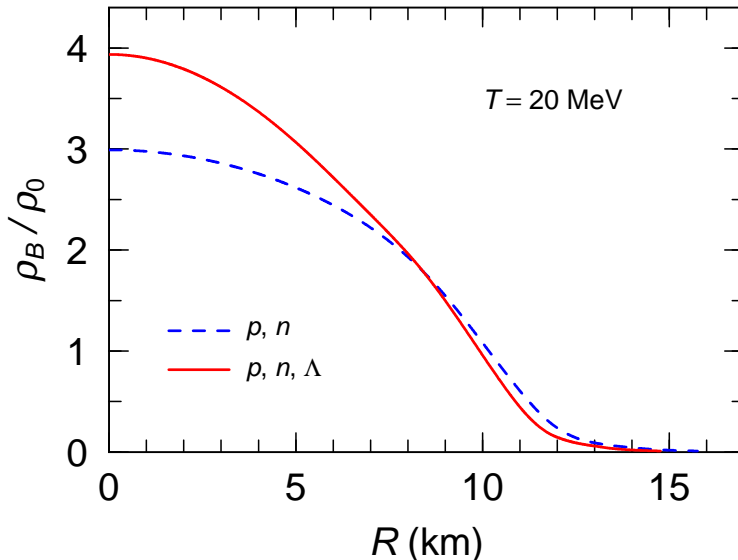


FIG. 14: (Color online) PNS Density distribution versus radius. Solid and dashed lines represent the results with and without  $\Lambda$ s at  $T = 20$  MeV, respectively.

### 4. Momentum transfer

We use these density distributions of the PNS to the calculation of the neutrino momentum transport. We define the effective spherical surface  $S_N$  where  $\rho_B = \rho_0$ , and estimate



the kick velocity from the angular dependence of the emitted neutrino momentum at this surface. The total momentum per unit time of the neutrinos emitted along the direction  $\mathbf{n}$  is then calculated as

$$P = \int_{S_N} d\mathbf{r} \int \frac{d^3k}{(2\pi)^3} \Delta f(\mathbf{r}, \mathbf{k}) (\mathbf{k} \cdot \mathbf{n}) \delta(\mathbf{k} - (\mathbf{k} \cdot \mathbf{n})\mathbf{n}) . \quad (71)$$

The momentum  $P$  can be approximately written as

$$P = P_0 + \Delta P \approx P_0 + P_1 \cos \theta \quad (72)$$

in terms of the polar angle  $\theta$ . The asymmetry of the neutrino momentum  $\Delta P/P_0$  is shown as a function of  $\theta$  in Fig. 15.

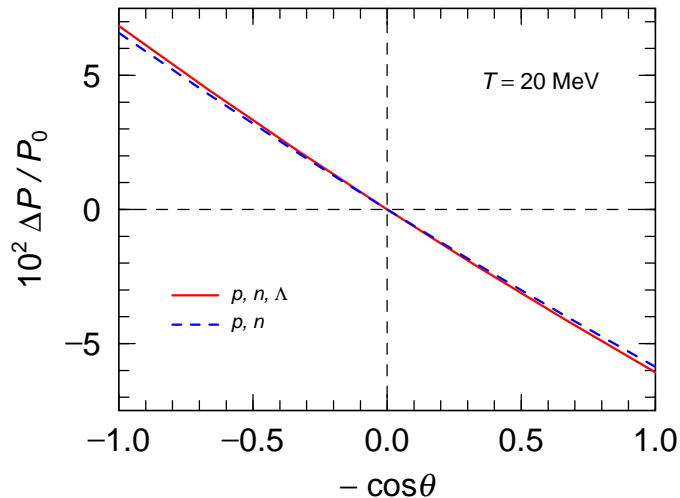


FIG. 15: (Color online) The variation of emitted neutrino momentum versus the polar direction. Solid and dashed lines represent the results in a system with  $\Lambda$ s and without  $\Lambda$ s at  $T = 20$  MeV, respectively.

We use the momentum distribution in Eq. (72) to calculate the ratio of the average momentum in the direction of the magnetic field  $\langle P_z \rangle$  to the total emitted neutrino energy  $E_T$ , *i.e.*  $\langle P_z \rangle / E_T = P_1/3P_0$ . Our results are estimated as  $\langle P_z \rangle / E_T = 0.0194$  and  $0.0176$  with and without the  $\Lambda$ s at  $T = 20$  MeV.

We assume that the total energy emitted in neutrinos is  $E_T \approx 3 \times 10^{53}$  erg [42]. For the  $M_{NS} = 1.68 M_\odot$  isothermal model with  $T = 20$  MeV, the calculated kick velocities are  $v_{kick} = \langle P_z \rangle / M_{NS} = 580$  km s $^{-1}$  or  $520$  km s $^{-1}$  in neutron-stars with or without  $\Lambda$ s, respectively.

In actual observations, the average value of the kick velocity is about  $v_{kick} = 400 \text{ km s}^{-1}$ , and the highest reported value is  $\sim 1500 \text{ km s}^{-1}$ . Our values are thus close to the observed average pulsar kick velocity. We note that Lai and Qian [42] obtained a similar result ( $v_{kick} = 280 \text{ km s}^{-1}$ ). However their result was calculated in a non-relativistic framework without  $\Lambda$  particles.

In the central region, high energy neutrinos up to  $E_\nu \gtrsim 100 \text{ MeV}$  are copiously produced, but their MFP is only about several  $10^3 \text{ cm}$ . They are, therefore, almost completely absorbed in the transport process. The average energy of the emitted neutrino is about  $20 \text{ MeV}$ , and most of neutrinos with energy  $< 50 \text{ MeV}$  contribute to the pulsar kick because the MFP for these neutrinos is larger (Fig. 12). If one presumes that the thermalization process is faster than the time scale at which the neutrino absorption process directly affects the collective motion of the PNS, then the cross-section in the low density region affects the final asymmetry of the neutrino emission.

Neutrinos are continuously further absorbed in the lower density regions before they are emitted outside the neutron-star, and the asymmetry should be retained. Indeed, when we extend the calculation to much lower density  $\rho_B = 0.5\rho_0$ , we find that the asymmetries are almost the same as the above results, but that the energy of the emitted neutrinos is small.

We caution, however, that in such low density regions, both the magnetic field and temperature may be lower than those assumed in the present isothermal model. If, instead of an isothermal neutron-star model, one were to use a an isoentropic model with uniform entropy, then the kick velocity may be smaller. In the surface region of magnetars, the magnetic field is still as high as  $10^{15} \text{ G}$ . That is, however, only about  $1/100$  of the value adopted in the present calculation. A lower magnetic field may reduce  $v_{kick}$ , but the lower density and temperature may enhance it. In such a subtle situation the scattering process which we ignored in the present calculation should also be included as it enhances the neutrino asymmetry. This could tend to increase the kick velocity.

## V. SUMMARY AND DISCUSSION

We have studied the neutrino scattering and absorption processes in strongly magnetized proto-neutron stars (PNSs) at finite temperature and density. We used a fully relativistic mean field (RMF) theory for the hadronic sector of the EOS including hyperons. We solved the Dirac equations for all constituent particles, p, n,  $\Lambda$ , e, and  $\nu$ , including a first order perturbation treatment of a poloidal magnetic field with  $B \sim 10^{17}\text{G}$ . We then applied the solutions to obtain a quantitative estimate of the asymmetry that emerges from the neutrino-baryon collision processes. We took into account the Fermi motion of baryons and electrons, the momentum dependence of their spin vectors, their recoil effects, and the associated energy difference of the mean fields between the initial and final particles exactly. We thus included the most important effects of the distortion of the Fermi spheres made by the magnetic field in this fully microscopic framework, i.e. the asymmetric neutrino scattering and absorption cross-sections.

We found that the differential neutrino absorption cross-sections are suppressed in the arctic direction parallel to the poloidal magnetic field  $\mathbf{B}$  in both cases with and without  $\Lambda$ s, while the differential scattering cross-sections are slightly enhanced. On the other hand, as expected from the sign of the couplings between the magnetic moments of baryons and the external field, the neutrino absorption and scattering cross-sections are respectively enhanced and suppressed in the antarctic direction. This is completely opposite to those in the arctic direction. The differential cross-sections were integrated over the momenta of the final electrons for absorption and over the momenta of initial neutrinos for the scattering, respectively. Quantitatively, when  $B = 2 \times 10^{17}\text{G}$ , the reduction for the absorption process is about 2%, and the enhancement for the scattering process is about 1% in the forward direction along the direction of  $\mathbf{B}$ .

Several interesting facts are evident in the angular distributions of both cross-sections, which depend on the magnetic field, the baryon density, and the temperature of the PNS matter. Among them, we find, an appreciable forward suppression and backward enhancement in the differential absorption cross-sections due to the difference in Fermi distributions between the spin-up and spin-down particles. This effect is larger at lower neutrino incident energy. The asymmetry becomes smaller as the density increases because the asymmetry arises from the magnetic part of the cross-sections which is proportional to the distortion

of the Fermi surfaces caused by the magnetic field. This tends to diminish with increasing matter density.

Using these cross-sections, we calculated the neutrino mean-free-paths (MFPs) as a function of the baryon density and temperature within a PNS. We then applied the above results to a calculation of pulsar-kicks in core-collapse supernovae. We solved the Boltzmann equation using a one-dimensional attenuation method, assuming that the neutrinos propagate along an approximately straight line and that the system is in steady state. We only included the MFPs for neutrino absorption which dominates over scattering in producing the asymmetric momentum transfer to the PNS.

We estimated pulsar kick velocities from the calculated total momentum per unit time that is transferred from the emitted neutrinos to the PNS along the direction parallel to the poloidal magnetic field  $\mathbf{B}$ . For a 20-MeV isothermal neutron-star with  $M_{NS} = 1.68M_{\odot}$  and a total energy in emitted neutrinos of  $E_T \approx 3 \times 10^{53}$ erg, the estimated kick velocities are  $v_{kick} = 580 \text{ km s}^{-1}$  and  $520 \text{ km s}^{-1}$  at  $T = 20 \text{ MeV}$ , including  $\Lambda$ s or no  $\Lambda$ s, respectively. These values are in reasonable agreement with the observed average pulsar-kick velocity of  $v_{kick} = 400 \text{ km s}^{-1}$ .

## VI. FUTURE WORK

In the present calculations we have adopted several assumptions which we summarize here both as a caveat for the reader and as a summary of issues to be addressed in future work. One such assumption is ignoring the neutrino scattering process in the solution of the Boltzmann equation. This scattering might enlarge the kick velocity. The one-dimensional attenuation method to solve the Boltzmann equation is also a coarse approximation. We have assumed that the asymmetry in neutrino emission is dominated by the emission from low-density regions with  $\rho_B \lesssim 3\rho_0$  where the neutrino opacity changes drastically. We have also assumed that the internal high-density region only contributes to the neutrino diffusive flux. This diminishes the expected neutrino asymmetry. However, as was discussed in the last section, if the thermalization process is considered dynamically the asymmetric neutrino scattering and absorption in the high-density region might also contribute to an aligned drift flux along the direction of  $\mathbf{B}$ . This could generate a gradual acceleration of the pulsar-kick. Numerical simulations of the neutrino transport inside a PNS coupled to our microscopic

calculations of the asymmetric neutrino scattering and absorption cross-sections are highly desirable in order to address to this critical question. It has been pointed out by Arras and Lai [41] that the neutrino distribution tends to be asymmetric only near the surface of PNS. This is consistent with the picture adopted in the present attenuation approximation for the neutrino transport. The issue becomes more subtle, however, if the thermalization process is considered. It would be interesting to clarify by numerical calculations the extent to which the asymmetric neutrino scattering and absorption contribute to the drift velocity as well as the diffusive velocity of outgoing neutrinos considered here. Other important questions are to address the link among asymmetric neutrino-baryon collisions, neutrino drift, and the collective response of the PNS to the pulsar kick. Further investigations must be done by numerically solving the Boltzmann equation for the neutrino transport inside a PNS without approximations, although we believe that our adopted scheme of attenuation is more or less consistent with the microscopic picture. Numerical calculations including several dynamical effects are now underway.

We also should take account of neutrino reactions in the much lower density region,  $\rho_B \gg \rho_0$ , although we did not include that in the present study because of the numerical difficulty in calculating thermodynamic quantities of the EOS in the RMF theory. In such low density regions, the magnetic field is weaker, but the width of the Landau level,  $\sqrt{2eB}$ , could be of the same order as the electron Fermi momentum, and it may affect the neutrino reactions.

The strength of the magnetic field inside the PNS can easily reach  $3 - 4 \times 10^{18}\text{G}$  in the high-density region according to the scalar virial theorem. This could make considerable effects, and a non-perturbative treatment of the magnetic field must be applied for this high field strength [59]. We may again need to take account of the Landau levels.

In this work we do not consider any magnetic contributions in the neutrino production [34–39]. This also makes a contribution to the asymmetry of neutrino emissions. As for the density profile of the PNS, we need to use an isoentropical model, in which the temperature becomes smaller in lower density region. This effect may enhance the kick velocity.

We also did not take account of the resonant spin-flavor conversion [60] in the magnetized PNSs, and the neutrino-flavor conversion due to the MSW effect [61] or the self-interaction effect [62] in the present calculations. All of these could alter the asymmetric neutrino emission. A quark-hadron phase transition [63] or a hyper-nuclear matter phase [64] un-

der a strong magnetic field is also considered to be another source to affect the neutrino asymmetry.

If a poloidal magnetic field exists in the progenitor stars for SNe, a stable toroidal magnetic field also is created in the core-collapse and explosion. In this case, the angular dependence of the neutrino reactions may show a more complicated and interesting behavior. Thus, there are many open questions to be addressed in the future studies which are beyond the scope of the present article.

## Appendix A: Dirac Spinor in a Magnetic Field

In this appendix, we explain the detailed expressions of the Dirac spinor under a magnetic field. The Dirac spinor  $u(p)$  can be obtained by solving the following Dirac equation

$$\hat{K}(p)u(p, s) \equiv [\not{p} - M - U_0(b) - U_T\sigma_z]u(p, s) = 0, \quad (\text{A1})$$

where  $U_T = \mu B$ . Here we defined the Green function  $S(p)$  as

$$\hat{K}(p)S(p) = 1. \quad (\text{A2})$$

Then the Green function is written as

$$S(p) = \det \hat{K} (S_0 + S_1 U_T + S_2 U_T^2 + S_3 U_T^3), \quad (\text{A3})$$

with

$$\begin{aligned} \det \hat{K} &= p_0^4 - 2p_0^2(\mathbf{p}^2 + M^2 + U_T^2) + (\mathbf{p}^2 + M^2)^2 + 2U_T^2(p_z^2 - \mathbf{p}_T^2 - M^2) + U_T^4, \\ S_0 &= (p_0^2 - E_p^2)(\not{p} + M), \\ S_1 &= (p_0^2 + E_p^2)\sigma_z + 2Mp_0\sigma_z\gamma_0 - 2p_z(\mathbf{p} \cdot \boldsymbol{\sigma})\gamma_0 \\ &\quad + 2Mp_z\gamma_5\gamma_0 + 2ip_0p_y\gamma^0\gamma^1 - 2ip_0p_x\gamma^0\gamma^2, \\ S_2 &= -p_0\gamma^0 + p_z\gamma^3 - p_x\gamma^1 - p_y\gamma^2 + M, \\ S_3 &= -\sigma_z. \end{aligned} \quad (\text{A4})$$

Here the single particle energy of this Dirac spinor, which is obtained from  $\det \hat{K} = 0$ , becomes

$$e(\mathbf{p}, s) = \sqrt{p_z^2 + \left(\sqrt{\mathbf{p}_T^2 + M^2} + sU_T\right)^2} = \sqrt{E_p^2 + 2sU_T\sqrt{\mathbf{p}_T^2 + M^2} + U_T^2}, \quad (\text{A5})$$

where  $s = \pm 1$ , and  $E_p = \sqrt{\mathbf{p}^2 + M^2}$ . Then,  $\det \hat{K}$  is rewritten as

$$\det \hat{K} = (p_0^2 - e^2(\mathbf{p}, 1))(p_0^2 - e^2(\mathbf{p}, -1)). \quad (\text{A6})$$

Furthermore, the Green function for this particle is written as

$$S(p) = \hat{K}^{-1}(p) = \sum_{s=\pm 1} \frac{u(\mathbf{p}, s)\bar{u}(\mathbf{p}, s)}{p_0 - e(\mathbf{p}, s) \pm i\delta} + \sum_{s=\pm 1} \frac{v(-\mathbf{p}, s)\bar{v}(-\mathbf{p}, s)}{p_0 + e(\mathbf{p}, s) + i\delta}, \quad (\text{A7})$$

where  $u(\mathbf{p}, s)$  and  $v(-\mathbf{p}, s)$  are the Dirac spinors of the positive and negative energy states, respectively.

By using the above quantities, we can obtain the Dirac spinor as

$$u(\mathbf{p}, s)\hat{u}(\mathbf{p}, s) = \lim_{p_0 \rightarrow e(\mathbf{p}, s)} (p_0 - e(\mathbf{p}, s))S(p) . \quad (\text{A8})$$

Now we expand  $S$  with respect to  $U_T$  and determine the Dirac spinor in first order perturbation theory. Here we define

$$D_e \equiv \lim_{p_0 \rightarrow e(\mathbf{p}, s)} \frac{p_0 - e(\mathbf{p}, s)}{\det \hat{K}} = \frac{1}{8e(\mathbf{p}, s) \left( sU_T \sqrt{\mathbf{p}_T^2 + M^2} \right)} . \quad (\text{A9})$$

When  $|U_T| \ll 1$ , we can substitute  $p_0 = e(\mathbf{p}, s) \approx E_p + sU_T \sqrt{\mathbf{p}_T^2 + M^2}/E_p$  into Eq. (A4) and obtain

$$\begin{aligned} D_e S_0 &\approx \frac{s}{4E_p} \left( 1 - \frac{sU_T \sqrt{\mathbf{p}_T^2 + M^2}}{E_p^2} \right) \left( 1 + \frac{sU_T}{2\sqrt{\mathbf{p}_T^2 + M^2}} \right) \\ &\quad \times \left\{ (\not{\mathbf{p}} + M) + \frac{sU_T \sqrt{\mathbf{p}_T^2 + M^2}}{E_p} \gamma_0 \right\} \\ &\approx \frac{1}{4E_p} \left\{ (\not{\mathbf{p}} + M) + \left[ \frac{\sqrt{\mathbf{p}_T^2 + M^2}}{E_p} \gamma_0 \right. \right. \\ &\quad \left. \left. + \frac{p_z^2 - \mathbf{p}_T^2 - M^2}{2E_p^2 \sqrt{\mathbf{p}_T^2 + M^2}} (\not{\mathbf{p}} + M) \right] sU_T \right\}_{p_0=E_p} \end{aligned} \quad (\text{A10})$$

$$\begin{aligned} U_T D_e S_1 &\approx \frac{s}{8E_p \sqrt{\mathbf{p}_T^2 + M^2}} \left( 1 - \frac{sU_T \sqrt{\mathbf{p}_T^2 + M^2}}{E_p^2} \right) \\ &\quad \times \left\{ S_1 + 2(E_p \sigma_z + M \gamma_0 \sigma_z + ip_y \alpha_x - ip_x \alpha_y) \frac{s \sqrt{\mathbf{p}_T^2 + M^2}}{E_p} U_T \right\}_{p_0=E_p} \\ &\approx \frac{1}{4E_p} \left\{ \frac{S_1}{\sqrt{\mathbf{p}_T^2 + M^2}} \right. \\ &\quad \left. + U_T \left[ -\frac{S_1}{2E_p^2} + \frac{1}{E_p} (E_p \sigma_z + M \gamma_0 \sigma_z + ip_x \sigma_x - ip_y \sigma_y) \right] \right\}_{p_0=E_p} \\ &\approx \frac{1}{4E_p} \left\{ s(\not{\mathbf{p}} + M) \gamma_5 \not{\mathbf{p}} + \frac{p_z}{E_p^2} (\beta \boldsymbol{\sigma} \cdot \mathbf{p} - M \gamma_5) U_T \right\}_{p_0=E_p} \end{aligned}$$

$$U_T^2 D_e S_2 \approx \frac{sU_T}{8E_p \sqrt{\mathbf{p}_T^2 + M^2}} (-E_p \gamma^0 + M + p_z \gamma^3 - p_x \gamma^1 - p_y \gamma^2) , \quad (\text{A11})$$

with

$$a = \frac{1}{\sqrt{\mathbf{p}_T^2 + M^2}} (p_z, 0, 0, E_p) . \quad (\text{A12})$$



Then, the Dirac spinor is written as up to the first order in  $U_T$

$$u(\mathbf{p}, s)\bar{u}(\mathbf{p}, s) \approx \frac{(\not{\mathbf{p}} + M)(1 + \gamma_5\not{\mathbf{p}}s)}{4E_p} + \frac{p_z U_T}{4E_p^3} (\boldsymbol{\sigma} \cdot \mathbf{p} - M\gamma_5\gamma_0) \\ + \frac{sU_T}{8E_p\sqrt{\mathbf{p}_T^2 + M^2}} (-E_p\gamma^0 + M + p_z\gamma^3 - p_x\gamma^1 - p_y\gamma^2) \quad . \quad (\text{A13})$$

## Appendix B: Neutrino Reaction Cross-Sections

In this appendix, we derive Eqs. (41) and (49). We start from the product of leptonic and hadronic weak currents in Eq. (36). By considering the spin-dependence, we express the  $W_{BL}$  in Eq. (36) as follows

$$W_{BL} = W_0 + W_i s_i + W_f s_f + W_e s_l + W_2 s_i s_f + W_3 s_l s_i + W_4 s_l s_f. \quad (\text{B1})$$

Note that  $W_e$ ,  $W_3$  and  $W_4$  only appear when the final lepton is an electron.

When  $|\mu_b B| \ll \varepsilon_b - U_0(b)$ , the baryon Fermi distribution function can be expanded as

$$n_b(e_b(\mathbf{p}, s)) \approx n_b(E_b^*(\mathbf{p}) + U_0(b)) + n'_b(E_b^*(\mathbf{p}) + U_0(b))\Delta E_b(\mathbf{p})s, \quad (\text{B2})$$

and the electron distribution is written as

$$n_e(e_e(\mathbf{k})) \approx n_e(|\mathbf{k}|) + n'_e(\mathbf{k})\frac{m_e}{|\mathbf{k}|}\mu_e B s_l, \quad (\text{B3})$$

where  $n'_b(x) = \partial n_b(x)/\partial x$ . In addition, the energy delta-function in Eq. (35) is also expanded as

$$\delta(|\mathbf{k}_i| + e_i(\mathbf{p}_i, s_i) - e_l(\mathbf{k}_f, s_l) - e_f(\mathbf{p}_f, s_f)) \\ \approx \delta(|\mathbf{k}_i| + E_\alpha^*(\mathbf{p}_i) + U_0(\alpha) - |\mathbf{k}_f| - E_\beta^*(\mathbf{p}_f) - U_0(\beta)) \\ + \delta'(|\mathbf{k}_i| + E_\alpha^*(\mathbf{p}_i) + U_0(\alpha) - |\mathbf{k}_f| - E_\beta^*(\mathbf{p}_f) - U_0(\beta))\Delta E \quad , \quad (\text{B4})$$

where  $\delta'(x) \equiv \partial\delta(x)/\partial x$ , and

$$\Delta E = \Delta E_\alpha(\mathbf{p}_i)s_i - \Delta E_\beta(\mathbf{p}_f)s_f - \frac{m_e}{|\mathbf{k}|}\mu_e B s_l \delta_{l,e} \quad . \quad (\text{B5})$$

Here, we define the momentum transfer  $q = (q_0, \mathbf{q})$  as

$$q \equiv (|\mathbf{k}_i| - |\mathbf{k}_f| - \Delta U_0; \mathbf{k}_i - \mathbf{k}_f) \quad (\text{B6})$$

with  $\Delta U_0 = U_0(\beta) - U_0(\alpha)$ , and rewrite the energy delta-function as

$$\begin{aligned} & \delta(|\mathbf{k}_i| + E_\alpha^*(\mathbf{p}_i) + U_0(\alpha) - |\mathbf{k}_f| - E_f^*(\mathbf{p}_i + \mathbf{q}) - U_0(\beta)) \\ &= \delta(E_\alpha^*(\mathbf{p}_i) + q_0 - E_\beta^*(\mathbf{p}_i + \mathbf{q})) = \frac{E_\beta^*}{|\mathbf{p}_i||\mathbf{q}|} \delta(t - t_p) \quad , \end{aligned} \quad (\text{B7})$$

where  $t \equiv \mathbf{q} \cdot \mathbf{p}_i / (|\mathbf{q}||\mathbf{p}_i|)$ , and

$$t_p = \frac{2q_0 E_\alpha^*(\mathbf{p}_i) + q^2 + M_i^{*2} - M_\beta^{*2}}{2|\mathbf{q}||\mathbf{p}_i|} \quad . \quad (\text{B8})$$

Furthermore we write

$$\delta'(E_\alpha^*(\mathbf{p}_i) + q_0 - E_\beta^*(\mathbf{p}_i + \mathbf{q})) = \frac{1}{|\mathbf{p}_i||\mathbf{q}|} \delta(t - t_p) + \frac{E_\beta^{*2}}{\mathbf{p}_i^2 \mathbf{q}^2} \frac{\partial}{\partial t} \delta(t - t_p) \quad . \quad (\text{B9})$$

Note that the terms proportional to  $s_\kappa$  ( $\kappa = l, i, j$ ) vanish in Eq. (B5), and the  $W_{2,3,4}$  do not contribute to the final results to first order in  $\mu_b B$ . In view of this fact, we can further separate the magnetic part of the cross-section of Eq. (39) into two parts as

$$\Delta\sigma = \Delta\sigma_M + \Delta\sigma_{el}, \quad (\text{B10})$$

where the first and second terms are the contributions from the target particle and the outgoing electron, which appear only in the absorption ( $\nu_e \rightarrow e^-$ ) process. Detailed expressions of each term are presented at the Eqs.(41)  $\sim$  (50) in text.

## Acknowledgments

This work was supported by the Grants-in-Aid for the Scientific Research from the Ministry of Education, Science and Culture of Japan (20244035, 21540412), Scientific Research on Innovative Area of MEXT (20105004), and Heiwa Nakajima Foundation. This work was partially supported by the National Research Foundation of Korea (Grant No. 2011-0003188, 2011-0015467). Work at the University of Notre Dame (G.J.M.) supported by the U.S. Department of Energy under Nuclear Theory Grant DE-FG02-95-ER40934.

- 
- [1] D.B. Kaplan and A.E. Nelson, Phys. Lett. **B 175**, 57 (1986); **B 179**, 409(E) (1986).
  - [2] C.-H. Lee, G.E. Brown, D.-P. Min and M. Rho, Nucl. Phys. **A 585**, 401 (1995).

- [3] T. Tatsumi, Prog. Theor. Phys. Suppl. **120**, 111 (1995) and references cited therein.
- [4] C.H. Lee, Phys. Rep. **275**, 197 (1996).
- [5] M. Prakash, I. Bombaci, M. Prakash, P.J. Ellis, J.M. Lattimer, R. Knorren, Phys. Rep. **280**, 1 (1997).
- [6] V. Thorsson, M. Prakash and J.M. Lattimer, Nucl. Phys. **A 572**, 693 (1994);  
*ibid* **A 574**, 851 (E) (1994).
- [7] T. Maruyama, H. Fujii, T. Muto and T. Tatsumi, Phys. Lett. **B 337**, 19 (1994).
- [8] H. Fujii, T. Maruyama, T. Muto and T. Tatsumi, Nucl. Phys. **A 597**, 645 (1996).
- [9] N.K. Glendenning, Phys. Rep. **342**, 393 (2001).
- [10] G.E. Brown and H.A. Bethe, Astrophys. J. **423**, 659 (1994).
- [11] J.A. Pons, S. Reddy, P.J. Ellis, M. Prakash and J.M. Lattimer, Phys. Rev. **C 62**, 035803 (2000); Astrophys. J. **553**, 382 (2001).
- [12] T. Tatsumi and M. Yasuhira, Nucl. Phys. **A 653**, 133 (1999);  
M. Yasuhira and T. Tatsumi, Nucl. Phys. **A 690**, 769 (2001).
- [13] N. Yasutake, K. Kotake, M.A. Hashimoto and S. Yamada, Phys. Rev. **D 75**, 084012 (2007).
- [14] D.G. Yakovlev, A.D. Kaminker, O.Y. Gnedin and P. Haensel, Phys. Rep. **354**, 1 (2001).
- [15] G. E. Brown, K. Kubodera, D. Page and P. Pizzochero, Phys. Rev. **D 37**, 2042 (1988).
- [16] T. Tatsumi, Prog. Theor. Phys. **80**, 22 (1988).
- [17] H. Fujii, T. Muto, T. Tatsumi and R. Tamagaki, Nucl. Phys. **A 571**, 758 (1994);  
Phys. Rev. **C 50**, 3140 (1994).
- [18] D. Page and E. Baron, Astrophys. J. **254**, L17 (1990).
- [19] S. Tsuruta, Phys. Rep. **292**, 1 (1998).
- [20] N. Yasutake, and K. Kashiwa, Phys. Rev. **D 79**, 043012 (2009).
- [21] S. Reddy, M. Prakash and J.M. Lattimer, Phys. Rev. **D58**, 013009 (1998).
- [22] B. Paczyński, Acta. Astron. **41**, 145 (1992).
- [23] For a review, G. Chanmugam, Annu. Rev. Astron. Astrophys. **30**, 143 (1992).
- [24] A.G. Lyne and D.R. Lorimer, Nature **369**, 127 (1994).
- [25] R.E. Rothchild, S.R. Kulkarni and R.E. Lingenfelter, Nature **368**, 432 (1994).
- [26] A. Burrows et al., Astrophys. J. **640**, 878 (2006).
- [27] A. Marek and H.-Th. Janka, Astrophys. J. **694**, 664 (2009).
- [28] C.J. Horowitz and G. Li, Phys. Rev. Lett. **80**, 3694 (1998).

- [29] A. Vilenkin, *Astrophys. J.* **451**, 700 (1995).
- [30] G.S. Bisnovatyi-Kogan, *Astron. Astrophys. Trans.* **3**, 287 (1993).
- [31] R.F. Sawyer and A. Soni, *Astrophys. J.* **230**, 859 (1979).
- [32] B.L. Friman and O.V. Maxwell, *Astrophys. J.* **232**, 541 (1979).
- [33] D. Blaschke, G. Röpke, H. Schulz, A.D. Sedrakian and D.N. Voskresensky, *Mon. Not. R. Astron. Soc.* **273**, 596 (1995).
- [34] N.N. Chugai, *Sov. Astron. Lett.* **10**, 87 (1984).
- [35] O.F. Dorofeev, V.N. Rodionov and I.M. Ternov, *Sov. Astron. Lett.* **11**, 123 (1985).
- [36] E.M. Henley, M.B. Johnson, L.S. Kisslinger, *Phys. Rev. D* **76**, 125007 (2007).
- [37] L.S. Kisslinger, *Mod Phys. Lett. A* **22**, 2071 (2007).
- [38] K.V. Parfenov, *Sov. J. Nucl. Phys.* 48 (1988) 651; *ibid.* 49 (1989) 1126.
- [39] D.N. Voskresensky and A.V. Senatorov, *Sov. Phys. JETP* **63**, 885 (1986);  
A.V. Senatorov and D.N. Voskresensky, *Phys. Lett. B* **184**, 119 (1987).
- [40] J. Berdermann, D. Blaschke, H. Grigorian, D.N. Voskresensky, *Prog. in Part. and Nucl. Phys.* **57**, 223 (2006).
- [41] P. Arras and D. Lai, *Phys. Rev. D* **60**, 043001 (1999).
- [42] D. Lai and Y.-Z. Qian, *Astrophys. J.* **495**, L103 (1998) (erratum 501, L155).
- [43] A. Kusenko, G. Segre and A. Vilenkin, *Phys.Lett. B* **437** 359 (1998).
- [44] T. Maruyama, T. Kajino, N. Yasutake, M.K. Cheoun and C.Y. Ryu, *Phys. Rev. D* **83**, 081303(R) (2011).
- [45] B. D. Serot and J. D. Walecka, The relativistic Nuclear Many Body Problem. In J. W. Negele and E. Voigt, editors, *Adv.Nucl.Phys.* **Vol.16**, page 1, Plenum Press, 1986, and references therein.
- [46] B.D. Serot and J.D. Walecka, *Int. J. Mod. Phys. E* **6**, 515 (1997).
- [47] B. C. Clark, S. Hama, R. L. Mercer, L. Ray and B. D. Serot, *Phys. Rev. Lett.* **50** (1983) 1644;  
S. Hama, B. C. Clark, E. D. Cooper, H. S. Sherif and R. L. Mercer, *Phys. Rev. C* **41**, 2737 (1990).
- [48] J. A. Tjon and S. J. Wallace, *Phys. Rev. C* **36**, 1085 (1987).
- [49] D. Hirata, K. Sumiyoshi, B.V. Carlson, H. Toki, *Nucl. Phys. A* **609**, 131 (1996).
- [50] T. Maruyama, W. Cassing, U. Mosel, K. Weber, *Nucl. Phys. A* **573**, 653 (1994).
- [51] T. Maruyama, H. Shin, H. Fujii, T. Tatsumi, *Prog. Theo. Phys.* **102**, 809 (1999).

- [52] K. Tsushima, K. Saito, J. Haidenbauer and A.W. Thomas, Nucl. Phys. **A 630**, 691 (1998);  
K. Saito, K. Tsushima and A.W. Thomas, Phys. Rev. **C55**, 2637 (1997);  
K. Saito and A.W. Thomas, Phys. Rev. **C 51**, 2757 (1995).
- [53] P.B. Demorest, T. Pennucci, S.M. Ransom, M.S.E. Roberts, J.W.T. Hessels, Nature **467**, 1081 (2012).
- [54] I. Bednarek, P. Haensel, J.L. Zdunik, M. Bejger and R. Manka, e-Print: arXiv:1111.6942 [astro-ph.SR] (2011).
- [55] H. Noumi, et al., Phys. Rev. Lett. **89**, 072301 (2002).
- [56] C.Y. Ryu, C.H. Hyun, S.W. Hong, B.T. Kim, Phys. Rev. **C75**, 055804 (2007).
- [57] C.Y. Ryu, T. Maruyama, T. Kajino, G.J. Mathews and M.K. Cheoun, Phys. Rev. **C85**, 045803 (2012).
- [58] E.E. Kolomeitsev and D.N. Voskresensky, Phys. ReV. **C68**, 015803 (2003).
- [59] C.Y. Cardall, M. Prakash, and J.M. Lattimer, Astrophys. J. **554**, 322 (2001).
- [60] T. Yoshida et al., Phys. Rev. **D80**, 125032 (2009).
- [61] A. Kusenko and G. Segre, Phys. Rev. Lett. **77**, 4872 (1996).
- [62] H. Duan, G.M. Fuller, J. Carlson, Y.-Z. Qian, Phys. Rev. **D74**, 105014 (2006).
- [63] D.P. Menezes, M. BenghiPinto, S.S. Avancini, C. Providência, Phys. Rev. **C80**, 065805 (2009).
- [64] A. Rabhi and C. Providência, J. Phys. **G37**, 075102 (2010).